

# Oriented Magnetite Inclusions in Plagioclase: Implications for the Anisotropy of Magnetic Remanence

Olga Ageeva<sup>1</sup>, Gerlinde Habler<sup>2</sup>, Stuart A. Gilder<sup>3</sup>, Roman Schuster<sup>4</sup>, Alexey Pertsev<sup>5</sup>, Olga Pilipenko<sup>6</sup>, Ge Bian<sup>2</sup>, and Rainer Abart<sup>2</sup>

<sup>1</sup>University of Vienna, Department of Lithospheric Research

<sup>2</sup>University of Vienna

<sup>3</sup>Ludwig Maximilians University

<sup>4</sup>Institute of Materials Science and Technology, TU Wien

<sup>5</sup>Institute of Geology, Ore Deposits, Petrography, Mineralogy and Geochemistry, Russian Academy of Sciences

<sup>6</sup>Institute of Earth Physics

November 24, 2022

## Abstract

Micron to sub-micron sized ferromagnetic inclusions in rock forming silicate minerals may give rise to particularly stable remanent magnetizations. When a population of inclusions have a preferred crystallographic or shape orientation in a rock, the recorded paleomagnetic direction and intensity may be biased by magnetic anisotropy. To better understand this effect, we investigated plagioclase grains from oceanic gabbro dredged from the Mid-Atlantic Ridge at 11-17N. The plagioclase grains contain abundant needle and lath shaped magnetite inclusions aligned along specific directions of the plagioclase lattice. Electron back scatter diffraction and anisotropy of magnetic remanence measurements are used to correlate the orientation distribution of the magnetite inclusions in the host plagioclase that contains multiple twin types (Manebach, Carlsbad, Albite and Pericline) with the bulk magnetic anisotropy of the inclusion-host assembly. In unaltered plagioclase, the anisotropy ellipsoid of magnetic remanence has oblate shapes that parallels the plagioclase (010) plane. It is suggested that recrystallization of magnetite inclusions from hydrothermal alteration shifts the relative abundance of the inclusions pertaining to the different orientation classes. We show that the maximum axis of the anisotropy ellipsoid of magnetic remanence parallels the plagioclase [001] direction, which in turn controls the recorded remanent magnetization direction. Our results are relevant for paleointensity and paleodirection determinations and for the interpretation of magnetic fabrics.

# **Oriented Magnetite Inclusions in Plagioclase: Implications for the Anisotropy of Magnetic Remanence**

O. Ageeva<sup>1,2</sup>, G. Habler<sup>1</sup>, S.A. Gilder<sup>3</sup>, R. Schuster<sup>4</sup>, A. Pertsev<sup>2</sup>, O. Pilipenko<sup>5</sup>, G. Bian<sup>1</sup>, and R. Abart<sup>1</sup>

<sup>1</sup> University of Vienna, Department of Lithospheric Research, Althanstrasse, 14, 1090 Vienna, Austria.

<sup>2</sup> Institute of Geology, Ore Deposits, Petrography, Mineralogy and Geochemistry, Russian Academy of Sciences, IGEM RAS, Staromonetny 35, 119017, Moscow.

<sup>3</sup> Ludwig Maximilians University, Department of Earth and Environmental Sciences, Theresienstrasse 41, 80333 Munich, Germany.

<sup>4</sup> Christian Doppler Laboratory for Interfaces and Precipitation Engineering (CDL-IPE), Institute of Materials Science and Technology, TU Wien, A-1060 Wien, Austria

<sup>5</sup> Institute of Earth Physics, IPE RAS, B. Gruzinskaya Str., 10, 123242, Moscow

Corresponding author: Olga Ageeva ([olga.ageeva@univie.ac.at](mailto:olga.ageeva@univie.ac.at)) <https://orcid.org/0000-0002-0158-2749>

## **Key Points**

Plagioclase from oceanic gabbro contains needle shaped magnetite inclusions that render plagioclase grains ferromagnetic.

Most of the needle elongation directions lie within or near the plagioclase (010) plane leading to pronounced magnetic anisotropy.

It is argued that magnetic anisotropy changes from triaxial oblate to rotational prolate with hydrothermal alteration.

## Abstract

Micron to sub-micron sized ferromagnetic inclusions in rock forming silicate minerals may give rise to particularly stable remanent magnetizations. When a population of inclusions have a preferred crystallographic or shape orientation in a rock, the recorded paleomagnetic direction and intensity may be biased by magnetic anisotropy. To better understand this effect, we investigated plagioclase grains from oceanic gabbro dredged from the Mid-Atlantic Ridge at 11-17°N. The plagioclase grains contain abundant needle and lath shaped magnetite inclusions aligned along specific directions of the plagioclase lattice. Electron back scatter diffraction and anisotropy of magnetic remanence measurements are used to correlate the orientation distribution of the magnetite inclusions in the host plagioclase that contains multiple twin types (Manebach, Carlsbad, Albite and Pericline) with the bulk magnetic anisotropy of the inclusion-host assembly. In unaltered plagioclase, the anisotropy ellipsoid of magnetic remanence has oblate shapes that parallels the plagioclase (010) plane. It is suggested that recrystallization of magnetite inclusions from hydrothermal alteration shifts the relative abundance of the inclusions pertaining to the different orientation classes. We show that the maximum axis of the anisotropy ellipsoid of magnetic remanence parallels the plagioclase [001] direction, which in turn controls the recorded remanent magnetization direction. Our results are relevant for paleointensity and paleodirection determinations and for the interpretation of magnetic fabrics.

## Plain Language Summary

Understanding how the Earth's magnetic field has varied in the past depends on the recording fidelity of the remanent magnetization held within the magnetic minerals in rocks, with magnetite being the most common. Magnetite may occur as tiny inclusions in host minerals such as plagioclase, and when they do, they are particularly robust magnetic recorders. Plagioclase from mafic plutonic rocks often contain needle-shaped magnetite inclusions whose orientations are fixed along specific crystallographic directions of the plagioclase, which leads to extreme magnetic anisotropy. The anisotropy can significantly bias magnetic recording by deflecting the magnetization direction into the magnetic foliation plane or the lineation direction, which may be at high angles from the magnetic field direction. By combining optical and electron microscopy with magnetic measurements of individual magnetite bearing plagioclase grains, we show that different types of crystallographic twinning in plagioclase dictates differential crystallographic

orientation directions of the magnetite inclusions; the resultant anisotropic distribution of magnetite crystals in turn controls the direction of the magnetic remanence.

## 1 Introduction

The remanent magnetization of rocks is primarily carried by magnetite. In mafic intrusive rocks, magnetite may be present in the form of millimeter sized matrix grains and/or magnetite may be present as micron to sub-micron sized inclusions hosted within silicate phases. Due to their multidomain characteristics the magnetite grains in the matrix are easily re-magnetized and are poor recorders of the paleomagnetic field. In contrast, the silicate hosted inclusions typically fall into the single to pseudo single-domain size range and thus have very good magnetic recording properties (Feinberg et al., 2006a; Kent et al., 1978, Fleet et al., 1980; Davis, 1981; Dunlop and Özdemir, 2001; Renne et al., 2002; Lappe et al., 2011; Usui et al., 2015; Knafelc et al., 2019). They exhibit high coercivity and have particularly stable remanent magnetizations (Özdemir and Dunlop, 1997; Feinberg et al., 2005). In addition, the silicate-hosted magnetite inclusions are protected from fluid-mediated alteration by their host crystals. Silicate-hosted, magnetite inclusions are thus robust carriers of the natural remanent magnetizations in mafic intrusive rocks (Cottrell and Tarduno, 1999; Tarduno et al., 2006; Renne et al., 2002; Feinberg et al., 2005; Selkin et al., 2008; Xu et al., 1997; Gee et al., 2004; Biedermann et al., 2016; Usui et al., 2015).

Magnetic anisotropy influences paleomagnetic recording. Depending on their formation pathways, the silicate-hosted, magnetite inclusions may have different shapes, different crystallographic orientation relationships (CORs) or different shape orientation relationships (SORs) to their silicate host grains. When the magnetite inclusions have isometric shape and/or are randomly oriented, the magnetic anisotropy ellipsoid is isotropic, and the grain may serve as a bias-free recorder of the paleomagnetic field. If, however, the magnetite inclusions have needle or plate shapes with systematic SOR and/or COR to their silicate host crystal, the inclusions may have substantial magnetic anisotropy. In such cases, the remanent magnetization vector recorded by the inclusion-bearing silicate grain may deviate from the direction of the paleomagnetic field and bias the recorded direction and intensity (Hargraves, 1959, Fuller, 1960, Fuller, 1963, Rogers et al., 1979). Knowledge of the origin and extent of magnetic anisotropy is therefore crucial to correct and interpret paleomagnetic data (Anson and Kodama, 1987, Tauxe et al., 2008, Lowrie et al., 1986, Jackson et al., 1991a).

88 In pyroxene, needle-shaped magnetite inclusions typically have one, or rarely two, types  
89 of SOR and COR with respect to the host crystal (Fleet et al., 1980; Ageeva et al 2017; Bolle et  
90 al., 2021), which may give rise to single grain and bulk-rock magnetic anisotropy (Ferré 2002;  
91 Maes et al. 2008; O'Driscoll et al. 2015, Biedermann et al 2015; 2019, Hirt and Biedermann  
92 2019). Indeed, a correlation between the magnetic fabric and the alignment of pyroxene grains in  
93 layered igneous rocks has been observed (Gee et al., 2004; Selkin et al., 2014). In contrast, at  
94 least eight different SOR and COR types have been identified in plagioclase with magnetite  
95 inclusions (Sobolev, 1990; Feinberg et al., 2006b; Usui et al., 2015; Ageeva et al., 2016, 2020a),  
96 and their potential contribution to bulk magnetic anisotropy of magnetite bearing plagioclase is  
97 less clear (Biedermann et al 2016; Hirt and Biedermann, 2019).

98 In this study, we analyzed the SOR and COR of a multitude of needle and lath shaped  
99 magnetite inclusions in plagioclase grains from oceanic gabbros that were dredged from the Mid-  
100 Atlantic Ridge. The relative abundances of different SOR and COR types were compared with  
101 measurements of the anisotropy of magnetic remanence (AMR) of the magnetite bearing  
102 plagioclase grains. Based on the combined evidence, the influence of the orientation distribution  
103 of the needle and lath shaped magnetite inclusions on the magnetic signature of magnetite  
104 bearing plagioclase grains is discussed. Multiple twinning mechanisms in plagioclase complicate  
105 the links between the SOR and COR of magnetite inclusions in a plagioclase host. The shape  
106 orientations of the magnetite needles were thus investigated on the scale of single twins and on  
107 the scale of a plagioclase crystal comprising multiple twin domains. Inclusion orientations were  
108 observed with correlated optical microscopy and scanning electron microscopy (SEM) including  
109 crystal orientation analysis based on electron backscatter diffraction (EBSD). Finally, we discuss  
110 how the orientation of the magnetite inclusions hosted by twinned plagioclase grains may  
111 contribute to the bulk magnetic properties of gabbro and how the AMR ellipsoid correlates with  
112 the distribution of the magnetite inclusions.

## 113 **2 Materials and Methods**

### 114 **2.1 Geological background and sampling**

115 The studied gabbro samples were dredged during the 26th, 30th and 32nd cruises of the  
116 Research Vessel Professor Logachev (Cipriani et al., 2009; Beltenev et al., 2007; 2009). The  
117 samples were collected from gabbro-peridotite outcrops along the Mid-Atlantic Ridge (Table

ST1, Supplementary data). Dredge site L2612 is within a lithospheric section exposed by the Vema Transform Fault (Cipriani et al., 2009; Bonatti et al., 2009). Sites L30-277 and L32-101 are within oceanic core complexes (OCCs) at 13°N and 13°30'N in the footwalls of low-angle, large-offset extensional faults that are typical for slow-spreading ridges (Karson and Lawrence, 1997; MacLeod et al., 2009). See MacLeod et al. (2009), Ondreas et al. (2012), Pertsev et al. (2012), and Escartin et al. (2017) for more information on the geology of OCC 13°N and OCC 13°30'N. Samples 1514-17 and 1419-10 were dredged from the Ashadze complex (Table ST1, Supplementary data). Samples L30-277-7, L30-277-10, 1514-17, 1419-10 and L32-101-1 are regarded as gabbroic intrusions in peridotite.

## 2.2 Polarization microscopy

The shape orientations of the magnetite inclusions in plagioclase were obtained using transmitted light polarization microscopy on petrographic thin sections. In cuts approximately perpendicular to the albite twin boundaries, several orientation classes of the magnetite inclusions that play a role in the formation of magnetic anisotropy can be discerned based on the angles between the inclusion elongation direction and the albite twin boundary and between the inclusion elongation direction and the plane of the thin section cut. The procedure is described in the supplementary material and illustrated in Supplementary Figure S-I. For other cuts, optical measurements were performed using a universal stage. Thin sections of 26 samples were analyzed using these optical methods.

## 2.3 Anisotropy of magnetic remanence (AMR) and Alternating Field (AF) demagnetization

We drilled cylindrical cores from the bulk samples L32-277-7, 1514-17, 1419-10 4 mm in diameter and 3.5 mm in height, to achieve a height to diameter ratio of 0.88 making the sample void of shape anisotropy (Collinson, 1983). The sample was inserted into a non-magnetic wood insert and placed on the SushiBar at LMU Munich (Wack and Gilder, 2012), which can automatically demagnetize rocks with an alternating field (AF) and impart anhysteretic remanent magnetizations to measure the anisotropy of magnetic remanence (AMR) based on a homemade coil and a 2G Enterprises, Inc, superconducting magnetometer. The sample was first stepwise AF demagnetized using 11 steps of incrementally higher peak fields up to 90 mT. Next, the sample was subjected to a 12-direction, AMR protocol following Wack and Gilder (2012) using an AF

field that decayed from 90 to 0 mT with a 50  $\mu$ T bias field applied as the AF waveform decayed from 85 to 20 mT. The same AMR protocol was repeated three times to assess reproducibility. AMR tensors were calculated according to the projection method of Wack (2015).

## 2.4 Electron Backscatter Diffraction analyses (EBSD)

An EBSD study including crystal orientation point analyses and crystal orientation mapping was applied to samples L32-277-7, L32-277-10, L-30-1241, L-30-1249, L32-101-1, 1514-17, and 1419-10. EBSD analyses were performed on chemo-mechanically (Syton<sup>TM</sup>) polished and carbon-coated thin sections using an FEI Quanta 3D FEG instrument at the University of Vienna. The Schottky-type field-emission gun scanning electron microscope (FEG-SEM) is equipped with an Ametek-EDAX Digiview 5 EBSD camera (CCD sensor with max. 1392x1040 pixels) mounted at 5° elevation, and an Ametek-EDAX Apollo X silicon drift detector for energy-dispersive X-ray spectrometry (EDX). An OIM DC 7.3.1 SW was used for contemporaneous EBSD and EDX data collection and composition-assisted reindexing (ChI-Scan SW). EBSD and EDX analyses were collected with electron beam settings of 15 kV accelerating voltage and 4 nA probe current, while the sample was at a 70° stage tilt and 14 mm working distance.

Crystallographic orientations of magnetite inclusions and adjacent plagioclase host were collected as manually selected single point analyses using 2x2 EBSD camera binning, 237 msec exposure time for each image frame and averaging over 8 or 10 frames per image. Static and dynamic background subtraction filters and histogram intensity normalization were applied in order to maximize the contrast of the Kikuchi pattern. Hough-transform based band detection was performed at a binned pattern size of 140x140 pixels, 1° theta step size using the central 83-91% of the spherical Kikuchi pattern cross section, applying a 9x9 pixel convolution mask. For EBSD indexing 3-16 reflector bands at a minimum peak distance of 10 pixels in Hough space were used while allowing for 2° interplanar angle tolerance. The reliability of the orientation solution was checked for each analysis based on the number of band triplets and the angular misfit between the detected bands and the reference crystal structure.

In addition to the single point analyses, plagioclase orientations and their 2D distribution were determined by automated crystal orientation mapping (COM). Using an 8x8 EBSD camera binning and an exposure time of 25-26 milliseconds for collecting single image frames at an indexing rate of 33-38 points per second. Thus, crystal orientations from 14 x 8 millimeter sized

sample areas were automatically stitched from a 0.5 x 0.5 millimeter sized matrix of submaps. In certain regions of interest, EDX energy spectra were simultaneously collected for each datapoint of the COM. Subsequently, the EBSD dataset was reindexed by considering only datapoints that pertain to the particular major element composition of plagioclase using the OIM ChI-Scan tool. With this approach, the plagioclase orientations in 28 x 7-millimeter sized areas of 3 samples were determined at step sizes of 20 or 40 micrometers.

### 3 Results

#### 3.1 Mineralogy and petrography

Samples L-32-101-1, L2612-41, and L2612-49 were described in Pertsev et al. (2015), Ageeva et al. (2016; 2017) and Pertsev et al. (2021). Sample L32-101-1 is a coarse-grained gabbro-norite injected by fine-grained felsic stringers. The gabbro-norite consists of plagioclase (pl, 50 vol%), clinopyroxene (cpx, 20-30 vol%), orthopyroxene (opx, 20-30 vol%) and minor interstitial ilmenite (ilm, <1 vol%). The felsic stringers are mostly <2 mm wide with some parts broadened up to 5 mm. They are fine-grained with variable mineral modes from pl + qz + biotite (bt) to local cpx-rich and zircon (zrn)-rich plagiogranite micro-lithologies (Pertsev et al., 2021). Samples L2612-41 and L2612-49 are coarse-grained oxide gabbros consisting of pl, cpx, and minor opx. Original prismatic pyroxenes and tabular pl grains are rarely preserved due to deformation and partial replacement by late-stage minerals. Late-magmatic processes are manifest by intracrystalline deformation of primary minerals, overprinted porphyroclastic textures resulting from solid-state ductile flow, and crystallization of titanium-rich hornblende and interstitial Fe-Ti oxides. In sample L2612-41, hydrothermal processes locally produced fayalite coronas between magnetite and opx as well as cracks filled with hornblende enriched in Fe<sup>2+</sup> and Cl (Pertsev et al., 2015). Samples 1514-17 and 1419-10 are coarse- and medium-grained oxide gabbros, respectively, without signs of late magmatic or hydrothermal alteration.

Sample L30-277-7 is a gabbro-norite comprising plagioclase, pyroxene, amphibole, and minor Fe-Ti-oxides (<0.5 vol.%). The plagioclase is generally labradorite in tabular or rare subhedral 0.5–5 mm sized grains, which are clouded with abundant opaque inclusions. The anorthite contents range from An<sub>60</sub> in the cores to An<sub>46</sub> in the rims and along healed cracks. The plagioclase grains are typically twinned. Large plagioclase grains are divided into Manebach or Carlsbad twins and the different twin individuals usually show internal Albite or Albite-Pericline



209 twinning. Clinopyroxene and rarely orthopyroxene occur as prismatic and subhedral 3–5 mm  
 210 sized grains with a dense cleavage network. In cpx, lamellae of opx occur parallel to the (100)  
 211 plane and vice versa. Clinopyroxene contains less than about 5  $\mu\text{m}$  sized needle and lath shaped  
 212 magnetite inclusions and ilmenite plates. Locally, rare magnesio-hornblende replaces  
 213 clinopyroxene. In the rock matrix, up to about 1 mm sized ilmenite, magnetite and exsolved  
 214 titanomagnetite grains typically occupy interstitial positions between the rock-forming silicate  
 215 minerals. In places, pyroxene is partially replaced by actinolite indicating incipient low-  
 216 temperature hydrothermal alteration.

217 In most samples, the plagioclase hosted magnetite inclusions are represented by micron  
 218 to sub-micron sized needle- or lath shaped crystals with shape orientations following several  
 219 well-defined directions in the plagioclase host. The magnetite needles are typically less than 1  
 220  $\mu\text{m}$  wide and several tens of  $\mu\text{m}$  long, often terminating at plagioclase twin boundaries. The  
 221 magnetite inclusions show systematic SORs and CORs with the plagioclase host, where eight  
 222 different orientation classes can be discerned (Sobolev, 1990, Wenk et al., 2011; Ageeva et al.,  
 223 2016; 2020a). Samples L-32-1241 and L-32-1249 are special in that the magnetite inclusions are  
 224 present as relatively short needles, which are aligned parallel to a single crystallographic  
 225 direction in the plagioclase. The magnetite inclusions often contain ilmenite and rarely  
 226 ulvospinel lamellae, which usually represent less than 15 vol.%. In contrast, the magnetite  
 227 inclusions in samples L-32-1241 and L-32-1249 show complex magnetite-ilmenite- $\text{ulvospinel}$   
 228 intergrowths. In addition to the needle and lath shapes, the magnetite inclusions may be  
 229 isometric—these are referred to as *dust-like inclusions*.

### 230 3.2 Shape orientation relationships

231 More than 95% of the magnetite inclusions pertain to one of the eight *orientation classes*,  
 232 most of which were described in Ageeva et al. (2020a) (Fig. 1). Seven of these orientation  
 233 classes correspond to magnetite inclusions that are elongated parallel to the normal directions of  
 234 specific low-index lattice planes of plagioclase, including  $\text{pl}(112)\text{n}$ ,  $\text{pl}(\bar{3}12)\text{n}$ ,  $\text{pl}(150)\text{n}$ ,  $\text{pl}(1\bar{5}0)\text{n}$ ,  
 235  $\text{pl}(1\bar{1}2)\text{n}$ ,  $\text{pl}(\bar{3}\bar{1}2)\text{n}$ , and  $\text{pl}(100)\text{n}$ , where  $\text{pl}(\text{hkl})\text{n}$ -mt refers to a magnetite inclusion that is  
 236 elongated perpendicular to the  $\text{pl}(\text{hkl})$  lattice plane. The magnetite inclusions pertaining to these  
 237 orientation classes are referred to as *plane-normal type* inclusions. Sobolev (1990) described  
 238 several of the plane-normal inclusion types in plagioclase from a layered gabbro-norite intrusion.

The eighth orientation class is represented by magnetite inclusions that are elongated parallel to the pl[001] direction. Magnetite inclusions with this orientation were described by Sobolev (1990), Wenk et al. (2011), Biedermann et al. (2016) and Ageeva et al. (2020a). Very rarely, needles elongated parallel to the normal direction of the pl(010) plane are observed.

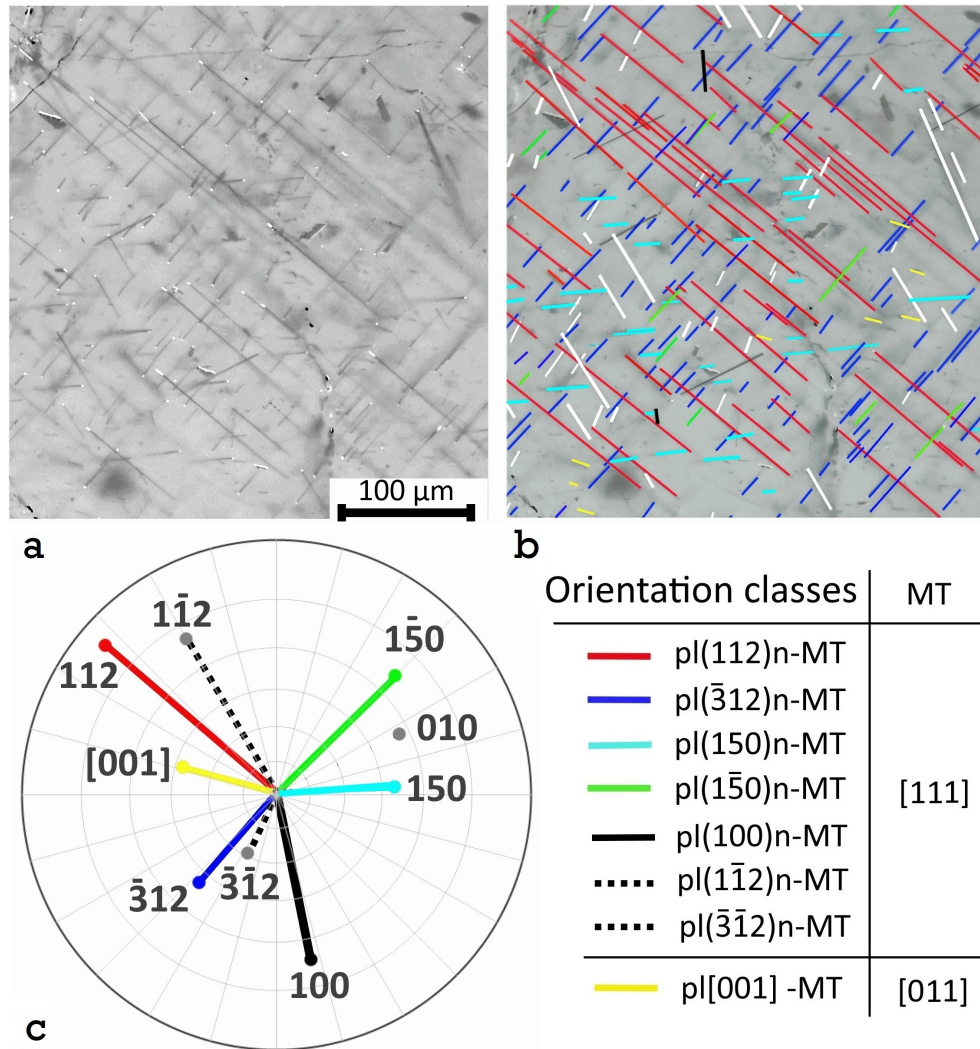


Figure 1. (a) Optical image under combined reflected and transmitted light showing magnetite inclusions in an untwinned domain of plagioclase in sample L32-277-10. (b) Same as in (a) with the magnetite needles color coded according to the orientation class they pertain to. (c) Pole figure of the needle orientations; note that the number of observed pl(112)n-mt needles is less than their true concentration due to their orientation subparallel to the plane of the thin-section.

### 3.3 Crystallographic orientation relationships

Ageeva et al. (2020a) demonstrated that the elongation direction of the plane-normal type magnetite inclusions is parallel to one of the mt(111) directions. In contrast, pl[001] inclusions

are elongated parallel to one of the  $mt[011]$  directions. All magnetite inclusions pertaining to the same orientation class are aligned parallel, with a maximum deviation of a few degrees from the average (Fig. 1). Crystallographic orientations of the magnetite needles show some rotational dispersion around the needle elongation direction. Figure 2 shows the distribution of the crystallographic orientations of  $pl(112)n$ - $mt$  needles in an untwinned plagioclase domain. The crystallographic orientations cluster at different positions pertaining to a rotation about the  $pl(112)$  pole (Fig. 2a). The clusters correspond to CORs where the magnetite  $mt(011)$  planes are parallel to low-index planes of plagioclase (Fig. 2 b). In some needles one of the  $mt[001]$  directions lie nearly parallel to the plagioclase  $[14\ 10\ 7]$  direction (Fig. 2c). According to Ageeva et al. (2020a), this orientation ensures a good fit of  $FeO_6$  octahedra of the magnetite crystal structure in channels in the plagioclase crystal structure running parallel to  $pl[001]$  and is referred to as *nucleation orientation*. The magnetite inclusions of other orientation classes show similar rotation and orientation clustering with respect to their elongation axis.

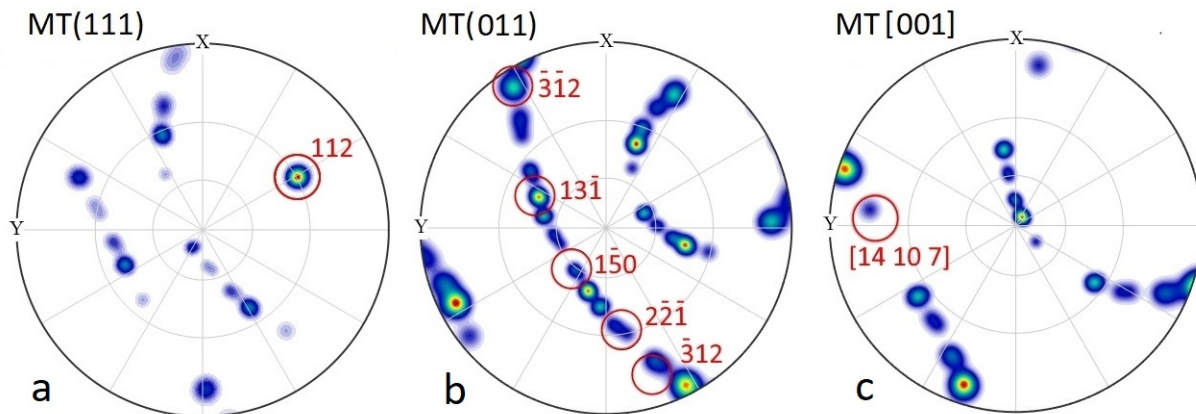


Figure 2. Stereographic projections showing the orientation distribution function (halfwidth=  $3^\circ$ ,  $N=17$ ) of  $pl(112)n$ - $mt$  inclusions in an untwinned domain of plagioclase (sample L30-277-10) for (a)  $mt(111)$ , (b)  $mt(011)$  and (c)  $mt[001]$ . Red circles and red labels indicate the orientations of crystallographic planes and directions of the plagioclase host. All symmetrically equivalent crystallographic planes of the cubic magnetite are shown. In this domain of the plagioclase grain, most needles cluster so that  $mt(011)$  is parallel to  $pl(13\bar{1})$ .

### 3.4 Crystallographic orientation relationships of dust-like magnetite inclusions

Apart from the needle and lath shaped magnetite inclusions, equant, or so-called *dust-like*, magnetite inclusions are present in the plagioclase host. As compared to the needle shaped magnetite inclusions, the dust-like inclusions generally have different and more variable CORs with respect the plagioclase host, but some preferred orientations can still be discerned. For

example, in the domain of the plagioclase grain shown in the Figure 1a dusty magnetite inclusions with  $mt(111)$  parallel to  $pl(120)$  dominate (Fig. 3). This type of inclusions also has two  $mt[001]$  directions parallel to the plagioclase directions  $pl[023]$  and  $pl[02\bar{3}]$ . Another type of COR that was often observed between the dust-like inclusions and plagioclase host is characterized by the parallel alignment of  $mt(111)$  and  $mt(110)$  with  $pl(010)$  and  $pl(100)$ , respectively.

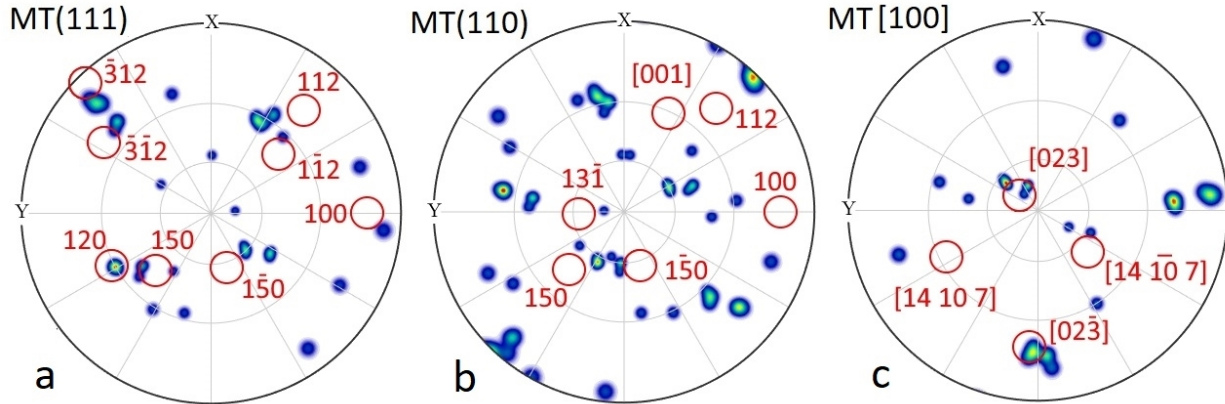


Figure 3. Stereographic projection showing the orientation distribution function (halfwidth=  $2^\circ$ ,  $N=15$ ) of the dust-like magnetite inclusion relative to the plagioclase grain shown in Figure 1a: (a)  $mt(111)$ , (b)  $mt(011)$  and (c)  $mt[001]$ . Red circles and labels indicate crystallographic planes and directions of the plagioclase host. Note, that no correspondence with the CORs of the needle-shaped inclusions is observed. Most dust-like inclusions have  $mt(111)$  parallel to  $pl(120)$ .

### 3.5 Shape orientation distribution of the magnetite inclusions

The magnetite inclusions pertaining to the different orientation classes are present in different proportions (Table 1). In most samples, except for those that experienced hydrothermal alteration (L-32-1241, L-32-1249), the inclusions of the  $pl(112)n$ - $mt$  class are the most abundant and represent  $\sim 50\%$  of all needle or lath shaped inclusions. The second most abundant inclusion type is represented by the  $pl(\bar{3}12)n$ - $mt$ , which represent up to 20% of the inclusions. The  $pl(\bar{1}50)n$ - $mt$  and  $pl(150)n$ - $mt$  inclusions together represent about 20%, and  $pl(\bar{3}\bar{1}2)n$ - $mt$  and  $pl(\bar{1}\bar{1}2)n$ - $mt$  together represent up to 10%.

The  $pl[001]$ - $mt$  inclusions are distributed heterogeneously. Some plagioclase grains host hardly any individuals of this type (Fig. 1), in other cases, they occur at moderate amounts (Figure 2 in Ageeva et al., 2020a). The  $pl[001]$ - $mt$  inclusions are the more typical inclusion type in the external parts of the plagioclase grains and in areas surrounding cracks. Moreover, this



inclusion type dominates samples that experienced hydrothermal alteration (L-32-1241, L-32-1249). The pl(100)n-mt inclusions also have quite heterogeneous distributions and usually accompany the pl[001]-mt inclusions (Figure 2 in Ageeva et al., 2020a).

The elongation directions of the magnetite inclusions from six out of the eight orientation classes lay approximately parallel to the pl(010) plane and form a  $\sim 30^\circ$  wide girdle distribution parallel to this plane (Fig. 4a). The most abundant inclusion types, pl(112)n-mt and pl( $\bar{3}12$ )n-mt plane normal type inclusions as well as the pl[001]-mt inclusions, which dominate in other domains, pertain to this girdle (Fig. 4a, b).

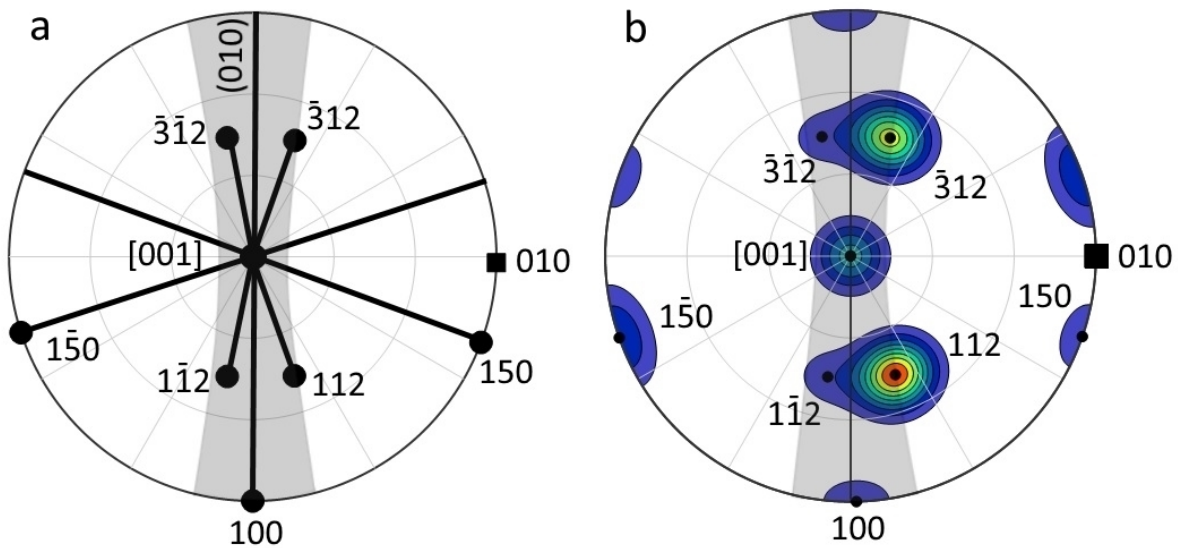


Figure 4. (a) Shape orientations of the magnetite inclusions of the different orientation classes in untwinned plagioclase viewed in a projection along the pl[001] direction. (b) Schematic orientation distribution inferred from statistical data (upper hemisphere). The  $30^\circ$  girdle parallel to the pl(010) plane (grey shaded area) comprises the pl(112)n-mt, pl( $\bar{3}12$ )n-mt, pl(100)n-mt, pl( $\bar{1}\bar{1}2$ )n-mt, pl( $\bar{3}12$ )n-mt, and of the pl[001]-mt type inclusions.

In sum, regardless of which orientation classes dominates, for 70-80% of the magnetite inclusions in plagioclase, the elongation direction closely parallels the pl(010) plane. The plagioclase grains in oceanic gabbro are typically twinned, and for understanding the potential influence of inclusion orientation anisotropy on the bulk magnetic properties of a magnetite bearing plagioclase grain, the orientation distribution of the magnetite needles needs to be considered in twinned plagioclase grains.

### 3.6 Shape orientation distribution of the magnetite inclusions in twinned plagioclase

Plagioclase grains in oceanic gabbro show complex twinning. Large grains typically follow a Manebach twin law (twin plane  $PL(001)$ ; twin axis  $PL(001)n$ ) and less frequently a Carlsbad law (twin plane  $\perp PL[001]$ ; twin axis  $PL[001]$ ). All grains show Albite-law, polysynthetic twinning (twin plane  $PL(010)$ ; twin axis  $PL(010)n$ ) or Albite and Pericline twins (twin plane  $\perp PL[010]$ ; twin axis  $PL[010]$ ) (Deer et al., 1966; Xu et al., 2016). Within a single plagioclase grain, the combination of the different twins leads to the formation of domains with different crystallographic orientations, which are related through the symmetry operations underlying the twinning. The dominance of some inclusion orientation classes in different twin individuals of plagioclase increases the observed dispersion of magnetite elongation directions inside a twinned plagioclase grain (Fig. 5).

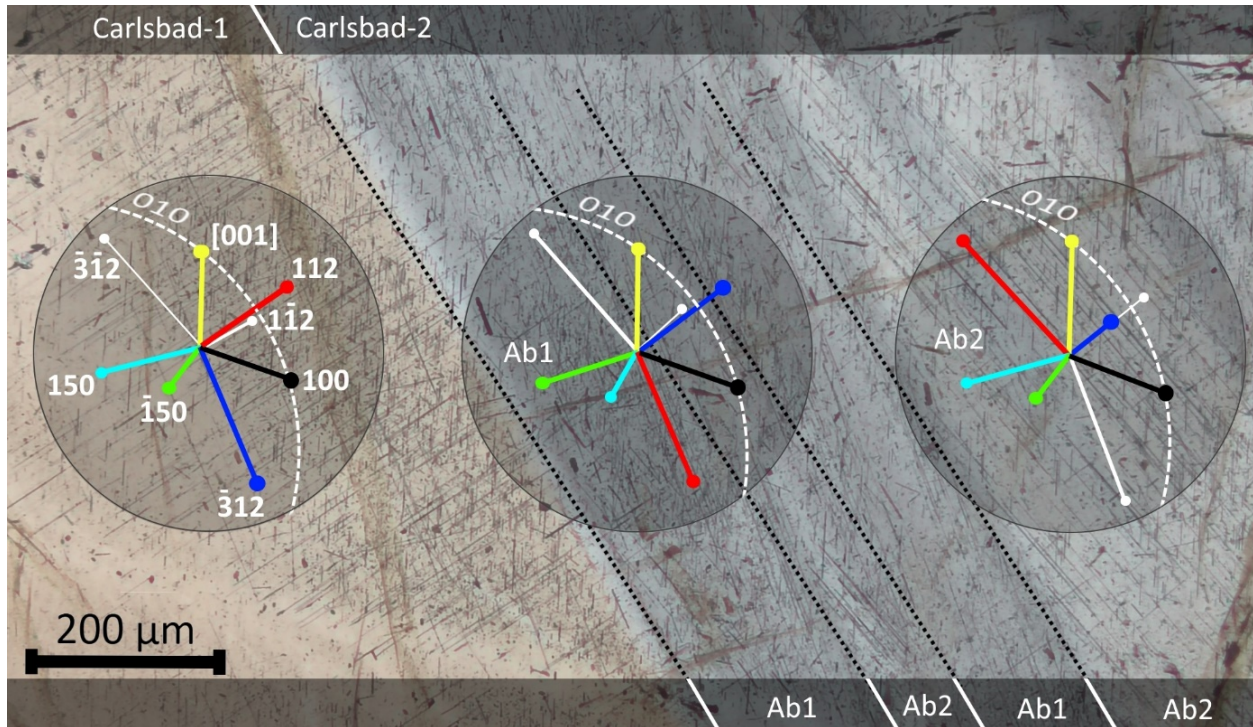


Figure 5. Transmitted plane-polarized light image of a twinned domain in plagioclase composed of Carlsbad-1 and -2 twins and albite twins (Ab1 and Ab2) in the Carlsbad-2 twin (Sample L30-277-7). The stereographic projections (upper hemisphere) show the different inclusion types. The needle directions are color coded according to their elongation directions (labeled in the left plot). The orientation of the twin boundaries is  $pl(010)$ —similar for all individual twins.

Based on the shape orientation distribution of the needle-shaped magnetite inclusions in untwinned plagioclase (Fig. 4), the shape orientation distribution of the magnetite needles in

twinned plagioclase was simulated for plagioclase grains with the most common twin combinations. The results are illustrated in Figure 6 and Figure S-II. The pl(010) plane orientation is barely affected by the twinning of plagioclase, and most of the inclusions contained in the twin individuals remain oriented closely parallel to the pl(010) plane so that the girdle distribution parallel to pl(010) persists even after multiple twinning.

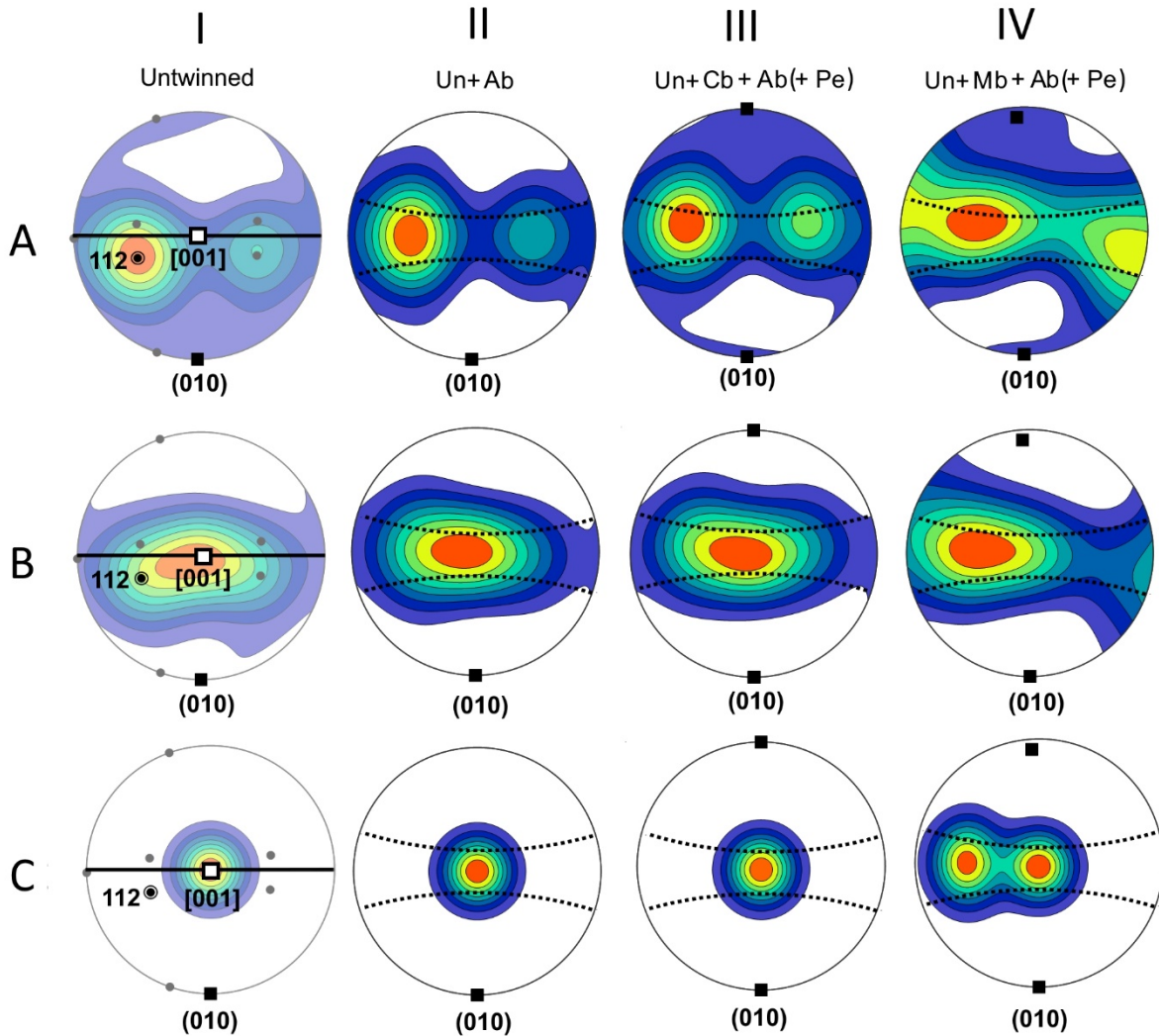


Figure 6. Schematic plots of inclusion orientation distributions showing simulated statistical distributions (halfwidth  $30^\circ$ ) of the magnetite needle orientations in plagioclase with different combinations of twinning (Ab - Albite, Pe - Pericline, Cb - Carlsbad, Mb - Manebach, Un - untwinned). In row (A), only magnetite inclusions of the plane-normal type, among which the pl(112)n-mt are the most abundant, are considered. In row (B), both, the plane-normal and the pl[001]-mt inclusion types are considered. In row (C) only the pl[001]-mt inclusions are considered. Table 1 lists the proportion of the inclusions pertaining to the different orientation classes. The  $30^\circ$  girdle parallel to the pl(010) plane (dashed black lines) comprises the inclusions oriented perpendicular to pl(112), pl( $\bar{3}$ 12), pl(100), pl( $\bar{1}$ 12) and pl( $\bar{3}$ 12) planes and parallel to



pl[001]. All plots have the same viewing direction along pl[001]. The poles of selected plagioclase planes and directions are shown for untwinned plagioclase in column I. The pole and the projection of the pl(010) plane are indicated by the black square and the thick black line, respectively; the pl[001] and pl(112)<sub>n</sub> directions are indicated by the white square and the black double circle, respectively; the gray dots mark the poles of the plane corresponding to the elongation directions of the other orientation classes. Combining pericline and albite twins hardly affects the orientation distribution of the magnetite inclusions. Cases III and IV consider combined albite and pericline twinning in Carlsbad and Manebach twin individuals. The MatLab MTEX software package (Krakow et al., 2007) performed the twinning operations and plotting.

In plagioclase that underwent high-temperature hydrothermal alteration, the majority of the inclusions are oriented along the pl[001] direction (Fig. 6, row C). It is worth noting that, since the pl[001] direction lies in the pl(010) plane, the magnetite inclusions are also elongated parallel to pl(010) in hydrothermally altered plagioclase. In cases with moderate (Fig. 6, row B) or low (Fig. 6, row A) concentrations of pl[001]-mt inclusions, all types of twinning show higher dispersion of the plane-normal-type inclusion orientations, yet have higher concentrations of pl[001]-mt inclusions. An additional maximum of pl[001]-mt orientations only results from Manebach twinning (Fig. 6, column IV, row C).

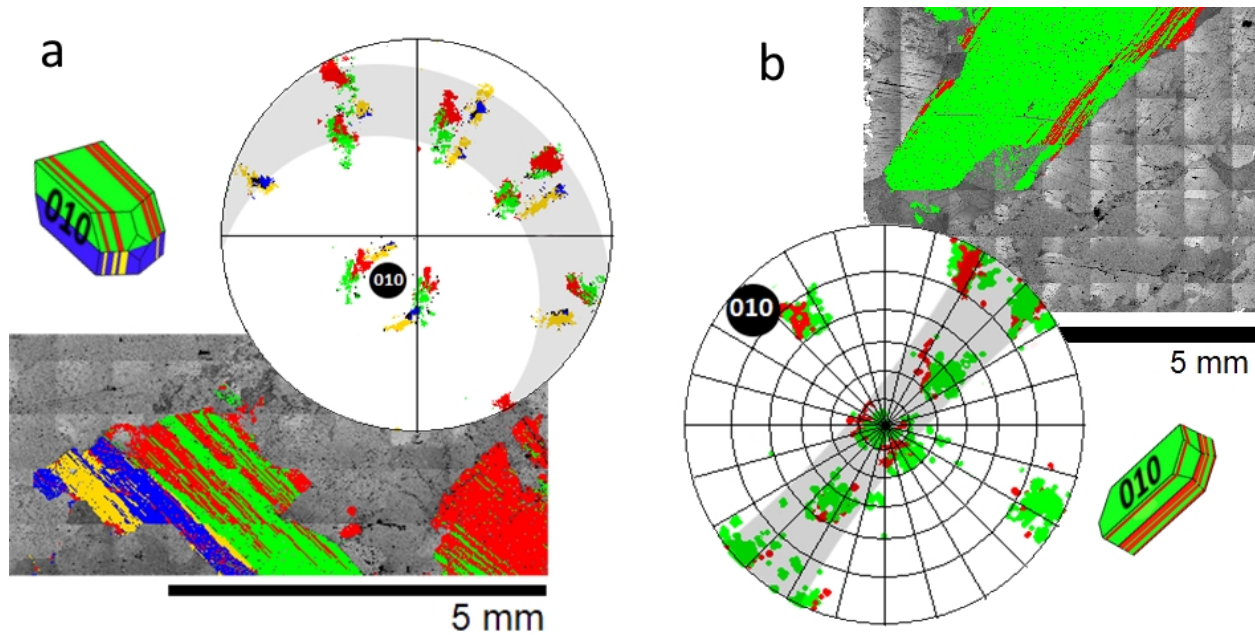


Fig. 7. EBSD data of L30-277-10 showing the poles of the plagioclase planes corresponding to the elongation directions of the needle-shaped magnetite inclusions of all eight orientation classes, and orientation maps corresponding to these projections. The plagioclase grains are twinned after (a) Manebach and Albite laws and (b) the Albite law. Models that schematically represent the mutual orientation relationships of the twins in plagioclase grains are shown. The



"30° girdle" containing the elongation directions of the majority of the needle shaped magnetite inclusions is shaded in gray. Black circles indicate the poles of the  $pl(010)$  planes. Supplementary Figure S-III gives more examples of CORs in twinned plagioclase. Note that the pole figures only show the inclusion elongation directions in grains of twinned plagioclase and do not include data on the statistical distribution of the inclusions.

EBSD data from plagioclase domains with Manebach and Albite twinning (Fig. 7a, Fig. S-III a, b), Carlsbad and Albite twinning (Fig. 7b, Fig. S-III c), exclusive polysynthetic Albite twinning (Fig. 7b), and Albite and Pericline polysynthetic twinning (Fig. S-III d) follow the simulated orientation relationships of the inclusions in untwinned and twinned plagioclase (Fig. 4 and 6). The combined evidence reveals an anisotropy in the shape orientations of the magnetite inclusions in twinned plagioclase, which may be described in terms of two end-member distribution types. First, in samples where the plane normal type inclusions dominate, the orientation distribution of the inclusions' elongation directions shows a minimum perpendicular to the  $(010)$  plane and a  $\sim 30^\circ$  wide girdle parallel to  $pl(010)$  that is relatively densely populated with needle elongation directions (row A in Fig. 6). The second end-member case occurs, when the magnetite inclusions oriented parallel to the  $pl[001]$  direction dominate. This type of orientation distribution is characterized by a maximum with elevated orientation densities around the  $pl[001]$  direction (row C in Fig. 6).

### 3.7 Anisotropy of magnetic remanence (AMR)

Figure 8 shows the AF demagnetization and anisotropy of magnetic remanence (AMR) of a plagioclase grain from sample L30-277-7 that is twinned after the albite law. The lattice orientations of the plagioclase and the magnetite inclusions were observed with polarized light (Figs. 8a-8b) and identified by EBSD (Figs. 8c-8d). AF demagnetization removed a very small fraction of the remanence, which we interpret as due to highly anisotropic magnetite (Fig. 8e). It is interesting to note that the maximum AMR axis lies subparallel to the  $pl[001]$ -direction and the minimum AMR axis coincides with the pole to the  $pl(010)$  plane, while the intermediate axis lies in the  $pl(010)$  plane (Fig. 8d). The anisotropy parameters define a triaxial prolate ellipsoid with a very high degree of anisotropy ( $P = 1.9$ ) (Table 2). The data reveal a good correspondence between the anisotropy of magnetic remanence and the distribution of the shape orientations of the needle-shaped magnetite inclusions. Stepwise demagnetization of the natural remanent magnetization shows that the magnetic remanence lies near the maximum ARM axis in the

pl(010) plane (Fig. 8d), thereby indicating substantial control of the plagioclase host on the magnetite inclusions, and hence on the bulk-rock remanent magnetization.

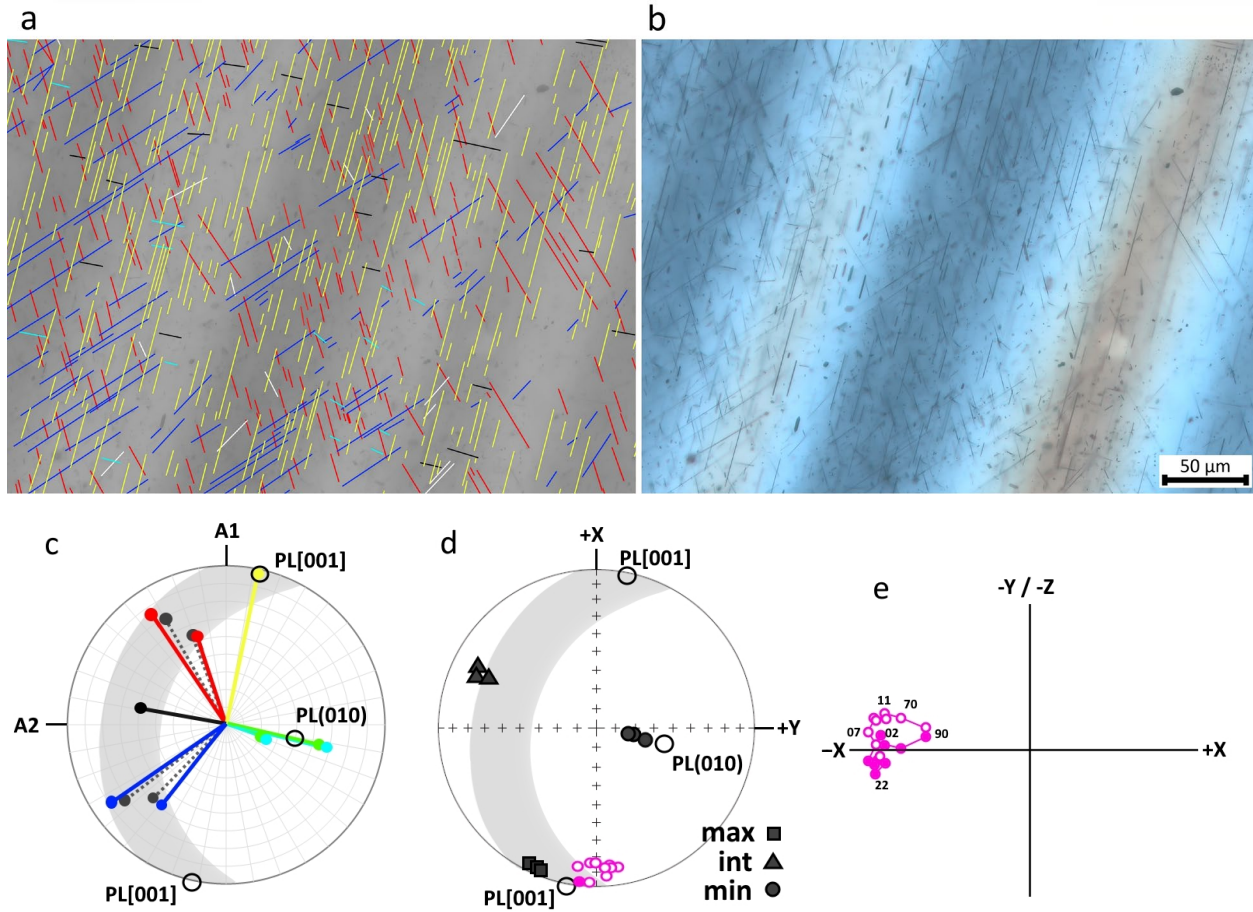


Figure 8. Confrontation of microscopy and magnetic measurements. Transmitted light optical images of sample L32-277-7 under crossed polarizers: (a) black and white, (b) real color - showing the magnetite inclusions in plagioclase. In (a) the different inclusion orientation classes are indicated as follows: pl(112)n-mt (red); pl( $\bar{3}$ 12)n-mt (blue); pl(150)n-mt and pl( $\bar{1}$ 50)n-mt (cyan) (this pair cannot be discerned due to a coincidence of their projections into the plane of the thin section); pl( $\bar{1}$ 12)n-mt and pl( $\bar{3}$ 12)n-mt (white); the latter two pairs cannot be discerned due to a coincidence of their projections in this thin section; pl(100)n-mt (black); pl[001]-mt (yellow). Both the pl( $\bar{1}$ 12)n-mt and pl( $\bar{3}$ 12)n-mt are indicated in white; c) Pole figure showing the shape orientations of the needles pertaining to the different orientation classes using the same color code as in (a) except for pl( $\bar{1}$ 12)n-mt and pl( $\bar{3}$ 12)n-mt, which are shown by dotted lines, and for pl( $\bar{1}$ 50)n-mt which is shown in green. The poles of the pl(010) and pl[001] directions are shown by open circles; the 30°-girdle parallel pl(010) is shaded in grey. (d) Stereographic projection of the pl[001] direction and the pl(010) pole of the plagioclase together with the maximum (max), intermediate (int), and minimum (min) AMR axes (the three symbols correspond to three repeated measurements, Table 2). The stereographic projection shows a good correlation between the minimum AMR axis with the pl(010) pole and the maximum AMR axis

with the  $pl[001]$  direction, while the AMR intermediate axis lies within the girdle of the poles defined by the magnetite inclusions in 8c. Pink circles are the individual directions from the AF demagnetization experiment, with the orthogonal plot shown in 8e. This shows that the remanence directions coincide well with the maximum AMR axis and the  $pl[001]$  direction. Open and filled circles represent poles in the upper and lower hemisphere, respectively. (e) Zijderveld plot showing the resistance to demagnetization (only ca. 30% of the total magnetization removed by 90 mT) and high coercivity of the grain.

A similar correspondence between the shape orientation distribution of the magnetite with respect to the plagioclase host and the anisotropy of magnetic remanence is observed for samples 1514-17 and 1491-10 (Fig. 9). The anisotropy parameters indicate triaxial prolate (Sample 1514-17) and triaxial oblate (Sample 1491-10) ellipsoids with anisotropy degrees of 1.7 and 4.3, respectively (Table 2). The minimum AMR axes and the  $pl(010)$  poles correlate well in both samples. The maximum AMR axes closely parallel the  $pl[001]$  direction in the plagioclase grain in 1514-17 (Fig. 9 a-c), represented by Albite twins and lies between the  $pl[001]$  directions of two Manebach twins in 1491-10 (Fig. 9 d-f). The natural remanent magnetization directions of these magnetite-bearing plagioclase grains again lie close to the maximum AMR axes.

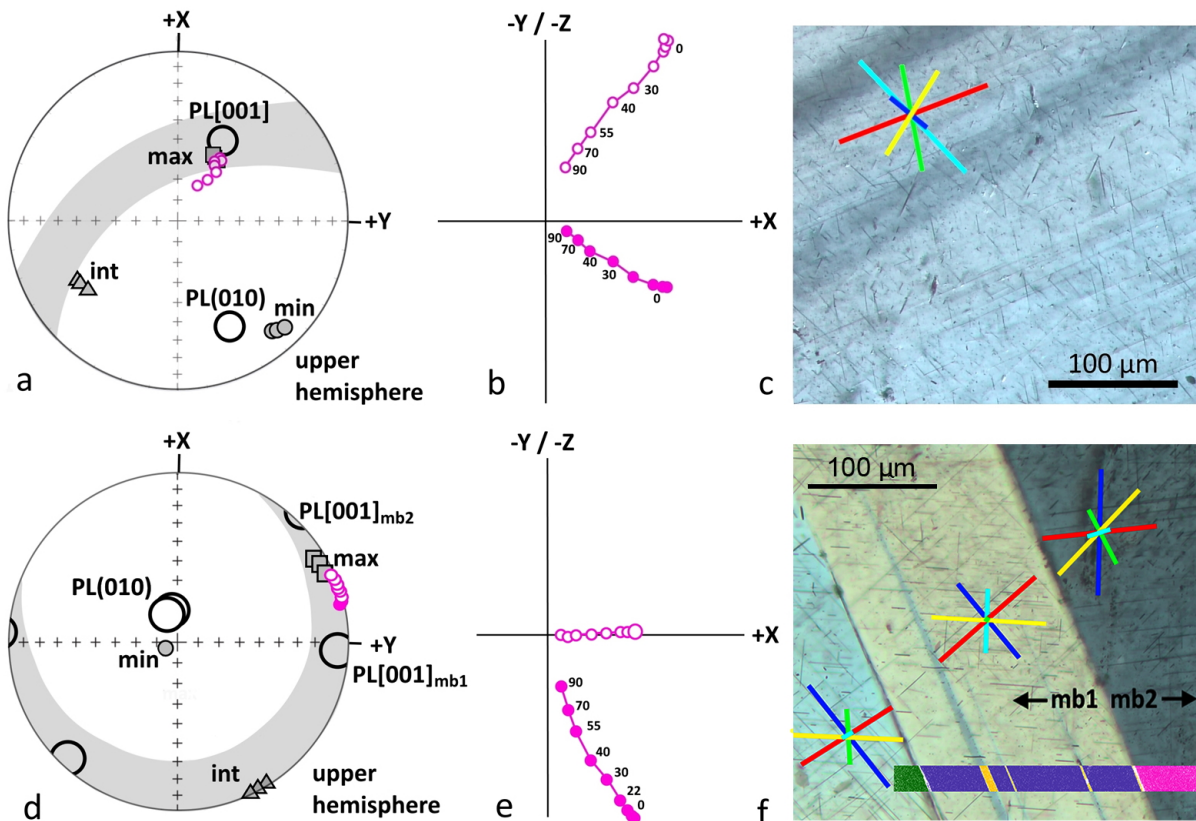


Figure 9. Crystallographic and magnetic orientation data for plagioclase grains from samples 1514-17 (a-c) and 1491-10 (d-f). (a,d) Stereographic projection showing the pl[001] direction and the pl(010) pole of the twinned plagioclase together with the maximum (max), intermediate (int), and minimum (min) AMR axes (the three symbols correspond to the three repeat measurements, Table 2). A good correlation exists between the minimum AMR axis with the pl(010) pole and the maximum AMR axis with the pl[001] direction in (a) and between the pl[001] directions of two Manebach twins labelled mb1 and mb2 in (d). The intermediate axes lie within or close to the 30°-girdle. The pink circles indicate the directions from the AF demagnetization experiment. (b, e) Zijderveld plots showing the demagnetization trajectory from 0 to 90 mT. (c, f) Transmitted light optical images (crossed polarizers) of the plagioclase grains with Albite (c) and Manebach combined with Pericline twinning (f). The orientations of the magnetite inclusions of the different orientation classes are indicated by colored lines: pl(112)n-mt (red); pl( $\bar{3}$ 12)n-mt (blue); pl(150)n-mt (cyan); pl( $\bar{1}$  $\bar{5}$ 0)n-mt (green); pl[001]-mt (yellow). The length of the lines is inversely proportional to the tilt of the inclusions relative to the surface of the thin section. Additional CORs data are in Figure S-IV (Supplementary data). The colored bar in figure “f” indicates the position of the orientation distribution map shown in Supplementary Figure S-IV.

## 4 Discussion

### 4.1 Inclusion origin

The plagioclase hosted magnetite inclusions of the studied samples most likely formed by exsolution from iron bearing plagioclase during the sub-solidus evolution of the gabbro (Usui et al., 2006, Bian et al. accepted). Based on the notion that the ilmenite lamellae that are frequently observed in the magnetite inclusions either formed by direct exsolution from Ti-magnetite at temperatures of about 900°C (Lattard, 1995; Lattard et al., 2005; Tan et al., 2016) or by high-temperature oxidation at temperatures in excess of 600°C (Tan et al., 2016), the formation temperature of the magnetite inclusions were above the Curie temperature of magnetite (573°C). The magnetic record of the magnetite inclusions and of the magnetite bearing plagioclase grains are thus considered as a thermoremanent magnetization. The ulvospinel lamellae present in the magnetite inclusions of samples L-32-1241, L-32-1249 indicate re-crystallization of these rocks at temperatures below about 600°C, which was probably linked to hydrothermal alteration (Ageeva et al., 2020b). In the following, we focus on the overall magnetic anisotropy of magnetite bearing plagioclase. In particular, we address the relationship between SOR and COR of the magnetite inclusions with the plagioclase host and the anisotropy of magnetic remanence of a magnetite-bearing plagioclase grain.

## 4.2 Orientation distribution of the inclusions in plagioclase

More than 95% of the needle-shaped magnetite inclusions belong to one of eight orientation classes including the seven plane-normal classes ( $\text{pl}(112)\text{n-mt}$ ,  $\text{pl}(\bar{3}12)\text{n-mt}$ ,  $\text{pl}(1\bar{1}2)\text{n-mt}$ ,  $\text{pl}(\bar{3}\bar{1}2)\text{n-mt}$ ,  $\text{pl}(100)\text{n-mt}$ ,  $\text{pl}(150)\text{n-mt}$ ,  $\text{pl}(1\bar{5}0)\text{n-mt}$ ), and the  $\text{pl}[001]\text{-mt}$  needles (Fig. 1, 2, 6). Six of these orientation classes, including the  $\text{pl}(112)\text{n-mt}$  inclusions, which are the most abundant, and the  $\text{pl}(1\bar{1}2)\text{n-mt}$  and  $\text{pl}(\bar{3}\bar{1}2)\text{n-mt}$  inclusions, which are the least common (Table 1, Fig. 1, 5b, 5), are elongated parallel or nearly parallel to the  $\text{pl}(010)$  plane and form a 30°-wide girdle parallel to the  $\text{pl}(010)$  plane (Fig. 4). Only the needles pertaining to the  $\text{pl}(150)\text{n-mt}$  and  $\text{pl}(1\bar{5}0)\text{n-mt}$  plane normal classes, which together constitute less than about 20% of the inclusions, have elongation directions at high angles to the  $\text{pl}(010)$  plane. Thus, more than 75% of the needle and lath-shaped magnetite inclusions pertain to the 30°-wide girdle parallel to the  $\text{pl}(010)$  plane (Fig. 3b, Table 1). The  $\text{pl}[001]\text{-mt}$  needles show independent behavior (Table 1) and represent the dominant or sole inclusion type in metamorphically and hydrothermally altered samples. A similar orientation distribution was reported from gabbro-norites by Sobolev (1990), where  $\text{pl}(112)\text{n-mt}$  or  $\text{pl}[001]\text{-mt}$  needles dominate.

Thus, the inclusions show a nearly planar orientation distribution parallel to the  $\text{pl}(010)$  plane with a maximum between the  $\text{pl}(112)$  pole and the  $\text{pl}[001]$  direction (Fig. 6, column I, rows A, B) or they show preferential alignment parallel to the  $\text{pl}[001]$  direction (Fig. 5, column I, row C).

## 4.3 Effect of plagioclase twinning

Four types of twins were identified in the plagioclase grains of the investigated gabbro (Fig. 4-7, Fig. S-I). The Manebach and Carlsbad twins all show signs of growth twinning (Seifert, 1964): the twinned plagioclase grains consist of two twin individuals of approximately similar size and shape and only occur in grains that are substantially larger than grains without such twinning.

The albite and pericline twins are polysynthetic and are regarded as transformation or deformation twins. Bian et al. (accepted) argued that the magnetite inclusions formed during or after transformation twinning. As a consequence, several shape orientation variants of the eight orientation classes may occur within a twinned plagioclase grain. The orientation distribution resulting from combining the different variants shows an increased dispersion of the SORs of the

inclusions (Fig. S-II), but for all combinations of twins the six orientation classes belonging to the 30°-girdle along the  $pl(010)$  plane remain within this girdle. The crystal orientation maps of the twinned plagioclase grains (Fig. 7, Fig. S-III) clearly reveal the girdle with high concentrations of inclusion elongation directions. The anisotropic distribution of needle-shaped magnetite inclusions with the preferred alignment of the inclusions parallel or sub-parallel to the  $pl(010)$  plane thus does not only exist in individual twin domains, but is also present in multiply twinned plagioclase grains. In addition, the orientation of the  $pl[001]$ -mt class of inclusions is invariant with respect to twinning after the Albite, Pericline and Carlsbad laws. This twinning thus increases the concentration of the  $pl[001]$ -mt inclusions relative to the needles of all other orientation classes the orientations of which become more dispersed through the twinning (Fig. S-II). As a consequence, in twinned plagioclase the anisotropy in the orientation distribution of the inclusions still has its minimum normal to the  $pl(010)$  plane and its maximum close to parallel to the  $pl[001]$  direction, or between the  $pl[001]$  direction and the normal to the  $pl(112)$  plane (Fig. 6 row A, columns II-IV).

The most important characteristics of the inhomogeneous distribution of needle elongation directions are the minimum density of orientations sub-perpendicular to the  $pl(010)$  plane and the maximum density of orientations sub-parallel to  $pl[001]$  direction, which is typical for the grains with moderate and high concentrations of  $pl[001]$ -mt inclusions. In cases where the plane normal type magnetite inclusions dominate, the maximum is shifted towards the normal of  $pl(112)$  plane, which is 45° away from the  $pl[001]$  direction, but still lies within the  $pl(010)$ -girdle.

#### 4.4 Magnetic anisotropy of magnetite-bearing plagioclase

Figures 8d and 9a,d show that the maximum AMR axis directions and the remanent magnetization directions are nearly parallel to the  $pl[001]$  direction. Thus, the orientation of the AMR ellipsoid is well aligned with the anisotropy of the inclusion orientation distribution, which has its maximum directed along  $pl[001]$  and the minimum perpendicular to the  $pl(010)$  plane. Moreover, the NRM vector directions lie close to the axis of maximum magnetization of the AMR ellipsoid (Fig. 8d, 9a,d); hence, the magnetic anisotropy controls the remanent magnetization recording. Usui et al. (2015) found a similar effect in plagioclase from Paleoproterozoic granitoids.

For oceanic gabbro, it is thus well established that the anisotropy of remanence of individual needle-shaped magnetite micro-inclusions is imprinted on the entire plagioclase-host grain through the anisotropic orientation distribution of the needle elongation directions. The plagioclase grains in mafic intrusive rocks are typically tabular parallel to  $pl(010)$  with their longest direction parallel to the  $pl[001]$  or  $pl[100]$  directions (Gee et al., 2004; Higgins, 2006). In foliated gabbro, the  $pl(010)$  plane is usually aligned parallel to the foliation plane (Feinberg et al., 2006b) and the  $pl[001]$  may coincide with the lineation direction (Gee et al., 2004). This gives rise to a *normal magnetic fabric*, which is characterized by a correspondence between the long and the short axes of the magnetic anisotropy ellipsoid and the directions of silicate petrofabric lineation and foliation, respectively (Rochette et al., 1992, Gee et al., 2004, Higgins, 2006; Selkin et al., 2014, Cheadle and Gee, 2017). The observed orientation distribution of the magnetite micro-inclusions in twinned plagioclase grains is in accordance with a magnetic fabric with the minimum magnetization normal to  $pl(010)$  and the maximum magnetization sub-parallel to  $pl[001]$ .

Alignment of minerals is typical for oceanic gabbros of fast spreading ridges, where the  $pl(010)$  plane is parallel to the foliation plane (Seront et al., 1993; Cheadle and Gee, 2017). Our gabbro samples come from a slow-spreading zone of the Mid Atlantic ridge and the studied material show no clear bulk mineral alignment. Given the magnetic anisotropy of the magnetite bearing plagioclase grains, a normal magnetic fabric would be expected to arise if mineral alignment occurred in foliated or lineated varieties of the oceanic gabbros. The plagioclase-hosted micro-inclusions may represent the single or the dominant carrier of magnetization, or alternatively, they may constitute the bulk rock magnetic fabric together with the magnetic fabric formed by micro-inclusion bearing pyroxene (Selkin et al., 2014; Biederman et al., 2016) and by the coarse-grained interstitial magnetite grains in the rock matrix (Stephenson, 1994; Feinberg et al., 2006b; Suhr et al., 2008, Uyeda et al., 1963).

The possible contribution of the plagioclase-hosted inclusions to the magnetic anisotropy may be estimated from routine petrographic observations with an optical microscope. The magnetite needles constituting the  $pl(010)$  girdle can be discerned from those that pertain to the orientation classes with the needle elongation directions at a high angle to the  $pl(010)$  plane by conventional polarization microscopy (Figure S-I, Supplementary data). The relative abundances of the needles belonging to the two groups allows one to estimate the degree of anisotropy in

their orientation distribution and to predict the AMR of the magnetite in a plagioclase grain. This method may be used to plagioclase with twinning according to the Albite law, which is typical in mafic rocks.

#### 4.5 Effect of hydrothermal alteration

In samples L-32-1241 and L-32-1249, all plagioclase-hosted magnetite inclusions are aligned parallel to the  $pl[001]$  direction and thus pertain to the single  $pl[001]$ -mt orientation class. These samples were affected by high-temperature hydrothermal alteration (Pertsev et al., 2015). Domains containing  $pl[001]$ -mt inclusions are typical for the rim zones of plagioclase grains or around cracks. A similar prevalence of  $pl[001]$ -mt inclusions was described from metamorphic rocks (anorthositic gneisses) by Wenk et al. (2011). We infer that magnetite inclusions of the  $pl[001]$ -mt type form over a wide range of conditions (late magmatic, metamorphic, hydrothermal, etc.), whereas the magnetite inclusions in the plane normal types appear to be restricted to late magmatic stages.

It should be noted that the inclusions of the plane-normal orientation classes are elongated parallel to one of their  $mt(111)$  directions, which are the easy axes of magnetization (Ageeva et al., 2020a; Bian et al., accepted). In contrast, the  $pl[001]$ -mt inclusions are elongated parallel to one of their  $mt(011)$  directions. Due to the fact that shape has a stronger influence on magnetic anisotropy than crystallographic direction (Rochette et al., 1992), this difference supposedly only plays a subordinate role.

In plagioclase domains with only  $pl[001]$ -mt inclusions, a rotational prolate shape is expected for the ellipsoid of the magnetic remanence anisotropy with the long axis parallel to the  $pl[001]$  direction for Carlsbad, albite and pericline twins (Fig. 5, row C, columns I-III) or sub-parallel to the  $pl[001]$  direction for Manebach twins (Fig. 5, row C, columns IV). As the  $pl[001]$  direction lies in the  $pl(010)$  plane, such magnetite-bearing plagioclase will form or contribute to a so-called “normal magnetic fabric”, which is characterized by a correspondence between the long and the short axes of AMS ellipsoids to the lineation direction and the normal to the foliation plane the of silicate petrofabric, respectively (Rochette et al., 1992, Gee et al., 2004, Higgins, 2006; Selkin et al., 2014, Cheadle and Gee, 2017).

The exclusive presence of  $pl[001]$ -mt inclusions may be related to high temperature hydrothermal alteration or metamorphic overprint. It is expected, that when the proportion of  $pl[001]$ -mt inclusions increases relative to the inclusions of the plane-normal type, the shape of



the ARM ellipsoid of magnetite bearing plagioclase grains changes from predominantly oblate to predominantly prolate. In foliated gabbro, the exclusive presence of pl[001]-mt inclusions may contribute to an oblate magnetic anisotropy, and in lineated gabbro, a prolate magnetic anisotropy will arise when the pl[001] direction is aligned parallel to the lineation.

#### 4.6 Dust-like inclusions

The equant, so-called *dust-like* magnetite inclusions often accompany needle-shaped inclusions or may be present as the only type of inclusions in some plagioclase domains. In plagioclase domains where dust-like and needle-shaped inclusions occur together, they show a multitude of CORs with respect to the plagioclase host, but one COR is usually dominant. In such domains, about 50% of the dust-like inclusions show mt(111) parallel to pl(120) (Fig. 2a) and usually have short prismatic shapes. The pl(120) planes have d-spacings of  $D_{(120)*2}=2.37$ , which is only slightly lower than the d-spacing of the pl lattice planes that are aligned with one of the mt(111) planes of the plane-normal type inclusions ( $d=2.40$ - $2.50$ ). They may thus form by the same mechanism as the inclusions of the plane-normal types, but the poorer match in d-spacing between mt(111) and pl(120) leads to more isometric shapes. In addition, two of the mt[001] directions are aligned with the plagioclase pl[023] and  $\text{pl}[0\bar{2}3]$  directions (Fig. 2c)—a feature which is reminiscent of the magnetite inclusions of the plane-normal classes. These directions are parallel to lines connecting pairs of oxygen atoms in channels of the plagioclase crystal structure running parallel to pl[001] which are separated by a distance that is similar to the spacing between oxygen atoms along the mt[001] direction and correspond to the orientation of the apexes of  $\text{FeO}_6$ -octahedra of the magnetite crystal structures ( $4.12$ - $4.36$  Å). Analogous alignments between the mt[001] and the pl[14 10 7] and  $\text{pl}[14 \bar{10} 7]$  directions were identified for needle-shaped magnetite inclusions of the plane-normal types and interpreted as suitable modes for the accommodation of  $\text{FeO}_6$ -octahedra in the crystal structure of plagioclase. The corresponding COR was thus referred to as the nucleation orientation of the magnetite inclusions in plagioclase (Ageeva et al., 2020a).

## 5 Conclusions

Plagioclase grains from oceanic gabbro dredged at the Mid Atlantic Ridge ( $11$ - $17^\circ\text{N}$ ) were analyzed with respect to the relationships between the shape orientation distribution of needle and lath shaped magnetite inclusions and the anisotropy of magnetic remanence. The

magnetite inclusions are single to pseudo single domain-sized and show systematic shape and crystallographic orientation relationships with the plagioclase host. In plagioclase from unaltered gabbro the needle elongation directions form a 30° wide girdle distribution parallel to the pl(010) plane. This distribution gives rise to a triaxial anisotropy ellipsoid with the direction of the minimum axis sub-perpendicular to the pl(010) plane and the maximum axis sub-parallel to the pl(010) plane, which corresponds to the most abundant needle orientations. The natural remanent magnetization vector is subparallel to the direction of the maximum AMR axis indicating that the anisotropy generated by the fabric of the needle shaped magnetite inclusions controls the paleomagnetic signal. In hydrothermally altered samples, most magnetite needles are oriented parallel to the pl[001] direction and the overall texture of the magnetite inclusions changes so that the resulting ellipsoid of remanent magnetization is expected to attain a rotational prolate shape with the maximum remanent magnetization parallel to pl[001]. The magnetic anisotropy of magnetite bearing plagioclase contributes to a normal magnetic fabric in foliated or lineated gabbro, where the plagioclase (010) plane is parallel to the foliation and the pl[001] direction is parallel to the lineation. Plagioclase hosted magnetite inclusions are particularly stable recorders of the paleomagnetic field. For paleomagnetic reconstructions it is, however, essential that the potential anisotropy effects resulting from the needle and lath-shaped magnetite inclusions are adequately accounted for. The distribution anisotropy can be estimated based on standard petrographic analyses.

## Acknowledgments

This work was supported by the Austrian Science Foundation Grant no. I 3998-N29, Russian Foundation for Basic Research, grant no. 18-55-14003, and Russian Basic Research Program (projects no. 121041500220–0).

**Table 1. Distribution of needle-shaped magnetite inclusions (%) according to orientation class with low (A), moderate (B) and high (C) proportions of pl[001]-mt inclusions (N= 20 studied grains).**

	A	B	C	“Pl(010) girdle”
pl(112)n-mt	40-45	35	0-5	+
pl( $\bar{3}$ 12)n-mt	25	15	-	+
pl(1 $\bar{5}$ 0)n-mt and pl(150)n-mt	15	2	-	-
pl( $\bar{3}$ 12)n-mt and pl(1 $\bar{1}$ 2)n-mt	10	3	-	+
pl(100)n-mt	0-5	5	-	+

pl[001]-mt	5	40	95-100	+
------------	---	----	--------	---

**Table 2. Magnetic anisotropy parameters of a plagioclase grains from Samples L30-277-7, 1514-17 and 1491-10**

Run	L $M_{\max}/M_{\text{int}}$	F $M_{\text{int}}/M_{\min}$	P $M_{\max}/M_{\min}$	Pj	T
Sample L30-277-7					
1	1.63	1.14	1.86	1.92	-0.57
2	1.66	1.15	1.90	1.97	-0.57
3	1.52	1.19	1.81	1.84	-0.41
Sample 1514-17					
1	1.47	1.19	1.75	1.77	-0.38
2	1.38	1.21	1.67	1.68	-0.25
3	1.40	1.19	1.67	1.68	-0.31
Sample 1491-10					
1	1.80	2.35	4.24	4.28	0.18
2	1.77	2.42	4.29	4.34	0.22
3	1.68	2.60	4.37	4.47	0.29

M – magnetization; L- degree of magnetic lineation; F – degree of magnetic foliation; P – degree of anisotropy; Pj – corrected degree of anisotropy; T – shape parameter (Tarling, Hrouda, 1993).

## References

- Ageeva, O., Habler, G., Pertsev, A., & Abart, R. (2017), Fe-Ti oxide micro-inclusions in clinopyroxene of oceanic gabbro: Phase content, orientation relations and petrogenetic implication. *Lithos* 290,104-115
- Ageeva O, Habler G, Topa D, Waitz T, Li C, Pertsev A, Griffiths T, Zhilicheva O, Abart R (2016) Plagioclase hosted Fe-Ti-oxide micro-inclusions in an oceanic gabbro-plagiogranite association from the Mid Atlantic ridge at 13°34'N. *American Journal of Science* 316(2). 85:109
- Ageeva, O., Bian, G., Habler, G., Pertsev, A., Abart, R. (2020a) Crystallographic and shape orientations of magnetite micro-inclusions in plagioclase. *Contributions to Mineralogy and Petrology*. 175(10). P 1-16.
- Ageeva, O., Pilipenko, O., Pertsev, A., & Abart, R. (2020b) Microstructure evolution of plagioclase-hosted Fe-Ti-oxide microinclusions in oceanic gabbro. In EGU General Assembly Conference Abstracts. p. 8851.
- Anson, G. L., & Kodama, K. P. (1987) Compaction-induced inclination shallowing of the post-depositional remanent magnetization in a synthetic sediment. *Geophysical Journal International*, 88(3), 673-692.
- Aranovich LY, Prokofiev VY, Pertsev AN, Bortnikov NS, Ageeva OA, Bel'tenev VE, Simakin, SG, (2015) Composition and origin of a K<sub>2</sub>O rich granite melt in the Mid Atlantic Ridge, 13 34' N: Evidence from the analysis of melt inclusions and minerals of the gabbro-plagiogranite association. *Doklady Earth Sciences* 460(2):174-178.

- Beltenev, V., Ivanov, V., Rozhdestvenskaya, I., Cherkashov, G., Stepanova, T., Shilov, V., Pertsev, A., Davydov, M., Egorov, I., Melekestseva, I., Narkevsky, E., Ignatov, V., 2007. A new hydrothermal field at 13° 30'N on the Mid-Atlantic Ridge. *InterRidge. News* 16, 9–10.
- Beltenev, V., Ivanov, V., Rozhdestvenskaya, I., Cherkashov, G., Stepanova, T., Shilov, V., Davydov, M., Laiba, A., Kaylio, V., Narkevsky, E., Pertsev, A., Dobretzova, I., Gustaytis, A., Popova, Y., Amplieva, Y., Evrard, C., 2009. New data about hydrothermal field on the Mid-Atlantic Ridge between 11° – 14°N: 32nd Cruise of R/V Professor Logatchev. *InterRidge News* 18, 14–18.
- Biedermann A.R., Pettke T., Angel R.J., Hirt A.M. Anisotropy of magnetic susceptibility in alkali feldspar and plagioclase // *Geophysical Supplements to the Monthly Notices of the Royal Astronomical Society*. 205(1). P. 479-489. 2016.
- Biedermann, A. R. (2020). Current challenges and future developments in magnetic fabric research. *Tectonophysics*, 228632.
- Biedermann, A. R., Bilardello, D., Jackson, M., Tauxe, L., & Feinberg, J. M. (2019). Grain-size-dependent remanence anisotropy and its implications for paleodirections and paleointensities—Proposing a new approach to anisotropy corrections. *Earth and planetary science letters*, 512, 111-123.
- Biedermann, A.R., Jackson, M., Chadima, M., Hirt, A.M., Feinberg, J.M., 2020. Beyond the second-order magnetic anisotropy tensor: higher-order components due to oriented magnetite exsolutions in pyroxenes, and implications for palaeomagnetic and structural interpretations. *Geophysical journal international* 223, 915-933.
- Bolle, O., Diot, H., Fransen, W., & Higgins, M. D. (2021). Central sagging of a giant mafic intrusion: the Ediacaran Sept Îles Layered Intrusion (Québec, Canada). *Journal of the Geological Society*, 178(1).
- Bonatti E., Brunelli D., Buck W.R., Cipriani A., Fabretti P., Ferrante V., Gasperini L. Ligi M. Flexural uplift of a lithospheric slab near the Vema transform (Central Atlantic): Timing and mechanisms // *Earth and Planetary Science Letters* 240(3-4). P. 642-655. 2005
- Chadima, Martin, Vladimír Cajz, and Patricie Týcová. "On the interpretation of normal and inverse magnetic fabric in dikes: examples from the Eger Graben, NW Bohemian Massif." *Tectonophysics* 466.1-2 (2009): 47-63.
- Cheadle, M. J., & Gee, J. S. (2017). Quantitative textural insights into the formation of gabbro in mafic intrusions. *Elements: An International Magazine of Mineralogy, Geochemistry, and Petrology*, 13(6), 409-414.
- Cipriani, A., Bonatti, E., Brunelli, D., & Ligi, M. (2009). 26 million years of mantle upwelling below a segment of the Mid Atlantic Ridge: The Vema Lithospheric Section revisited. *Earth and Planetary Science Letters*, 285(1-2), 87-95.
- Collinson, D.W. (1983), *Methods in Rock Magnetism and Paleomagnetism: Techniques and Instrumentation*, Chapman and Hall, New York, 503 pp.
- Cottrell, R. D., & Tarduno, J. A. (1999). Geomagnetic paleointensity derived from single plagioclase crystals. *Earth and Planetary Science Letters*, 169(1-2), 1-5.
- Davis, K. E. (1981). Magnetite rods in plagioclase as the primary carrier of stable NRM in ocean floor gabbros. *Earth and Planetary Science Letters*, 55(1), 190-198.

- 728 Dunlop, D. J., and Ö. Özdemir. *Rock magnetism: fundamentals and frontiers*. No. 3. Cambridge University Press,  
729 2001.
- 730 Escartín, J., Mevel, C., Petersen, S., Bonnemains, D., Cannat, M., Andreani, M., ... & Garcia, R. (2017). Tectonic  
731 structure, evolution, and the nature of oceanic core complexes and their detachment fault zones (13 20' N and 13 30'  
732 N, Mid Atlantic Ridge). *Geochemistry, Geophysics, Geosystems*, 18(4), 1451-1482.
- 733 Feinberg J.M., Wenk H.R., Scott G.R., Renne P.R. (b) Preferred orientation and anisotropy of seismic and magnetic  
734 properties in gabbro-norites from the Bushveld layered intrusion // *Tectonophysics* 420(3-4): 345-356. 2006b
- 735 Feinberg JM, Scott GR, Renne PR, Wenk HR Exsolved magnetite inclusions in silicates: Features determining their  
736 remanence behavior. *Geology* 33(6). P. 513-516. 2005
- 737 Feinberg, J. M., Harrison, R. J., Kasama, T., Dunin-Borkowski, R. E., Scott, G. R., & Renne, P. R. (2006a). Effects  
738 of internal mineral structures on the magnetic remanence of silicate-hosted titanomagnetite inclusions: An electron  
739 holography study. *Journal of Geophysical Research: Solid Earth*, 111(B12).
- 740 Ferré, E. C. (2002). Theoretical models of intermediate and inverse AMS fabrics. *Geophysical Research*  
741 *Letters*, 29(7), 31-1.
- 742 Fleet M.E., Gregory A.B., Robert L. Oriented magnetite inclusions in pyroxenes from the Grenville Province //  
743 *Canadian Mineralogist*. 18.1. P. 89-99. 1980
- 744 Fuller, M. D. (1963). Magnetic anisotropy and paleomagnetism. *Journal of Geophysical Research*, 68(1), 293-309.
- 745 Fuller, M.D., 1960. Anisotropy of susceptibility and the natural remanent magnetization of some Welsh slates.  
746 *Nature*, 186: 790–792.
- 747 Gee, J. S., Meurer, W. P., Selkin, P. A., & Cheadle, M. J. (2004). Quantifying three-dimensional silicate fabrics in  
748 cumulates using cumulative distribution functions. *Journal of Petrology*, 45(10), 1983-2009.
- 749 Gee, J. S., Meurer, W. P., Selkin, P. A., & Cheadle, M. J. (2004). Quantifying three-dimensional silicate fabrics in  
750 cumulates using cumulative distribution functions. *Journal of Petrology*, 45(10), 1983-2009.
- 751 Hirt, A. M., & Biedermann, A. R. (2019). Preferred orientation of ferromagnetic phases in rock-forming minerals:  
752 insights from magnetic anisotropy of single crystals. *Canadian journal of earth sciences*, 56(9), 994-1001.
- 753 Hargraves, R. B. (1959). Magnetic anisotropy and remanent magnetism in hemo-ilmenite from ore deposits at Allard  
754 Lake, Quebec. *Journal of Geophysical Research*, 64(10), 1565-1578.
- 755 Hargraves, R. B., D. Johnson, and C. Y. Chan, Distribution anisotropy: The cause of AMS in igneous rocks?  
756 *Geophys. Res. Lett.* 18, 2193-2196, 1991
- 757 Higgins, M. D. (2006). *Quantitative textural measurements in igneous and metamorphic petrology*. Cambridge  
758 university press.
- 759 Jackson, M. Anisotropy of magnetic remanence: a brief review of mineralogical sources, physical origins, and  
760 geological applications, and comparison with susceptibility anisotropy // *Pure and Applied Geophysics*. 136(1). P. 1-  
761 28. 1991a

- 762 Jackson, M. J., Banerjee, S. K., Marvin, J. A., Lu, R., & Gruber, W. (1991b). Detrital remanence, inclination errors,  
763 and anhysteretic remanence anisotropy: quantitative model and experimental results. *Geophysical Journal*  
764 *International*, 104(1), 95-103.
- 765 Karson, J. A., & Lawrence, R. M. (1997). Tectonic setting of serpentinite exposures on the western median valley  
766 wall of the MARK area in the vicinity of Site 920. In *PROCEEDINGS-OCEAN DRILLING PROGRAM*  
767 *SCIENTIFIC RESULTS* (pp. 5-22). National Science Foundation.
- 768 Kent, D. V., Honnorez, B. M., Opdyke, N. D., & Fox, P. J. (1978). Magnetic properties of dredged oceanic gabbros  
769 and the source of marine magnetic anomalies. *Geophysical Journal International*, 55(3), 513-537
- 770 Knafelc, J., Filiberto, J., Ferré, E. C., Conder, J. A., Costello, L., Crandall, J. R., ... & Schwenzer, S. P. (2019). The  
771 effect of oxidation on the mineralogy and magnetic properties of olivine. *American Mineralogist: Journal of Earth*  
772 *and Planetary Materials*, 104(5), 694-702.
- 773 Krakow R., Bennett R.J., Johnstone D.N., Vukmanovic Z., Solano-Alvarez W., Lainé S.J., Einsle J.F., Midgley  
774 P.A., Rae C.M.F., Hielscher R. On three-dimensional misorientation spaces // Royal Soc Mathe Phys Eng Sci.  
775 473(2206):20170274. 2017
- 776 Lappe, S. C. L., Church, N. S., Kasama, T., da Silva Fanta, A. B., Bromiley, G., Dunin-Borkowski, R. E., ... &  
777 Harrison, R. J. (2011). Mineral magnetism of dusty olivine: a credible recorder of pre-accretionary  
778 remanence. *Geochemistry, Geophysics, Geosystems*, 12(12).
- 779 Lattard D, Sauerzapf U, Kaesemann M (2005) New calibration data for the fe-ti oxide thermooxybarometers from  
780 experiments in the fe-ti-o system at 1 bar, 1,000-1,300 c and a large range of oxygen fugacities. *Contributions to*  
781 *Mineralogy and Petrology* 149(6).735-754
- 782 Lattard D. Experimental evidence for the exsolution of ilmenite from titaniferous spinel // *American Mineralogist*.  
783 80. P. 968–981. 1995
- 784 Lowrie, W., Hirt, A. M., & Kligfield, R. (1986). Effects of tectonic deformation on the remanent magnetization of  
785 rocks. *Tectonics*, 5(5), 713-722.
- 786 Maes, S. M., Ferré, E. C., Tikoff, B., Brown, P. E., & Marsh, J. S. (2008). Rock magnetic stratigraphy of a mafic  
787 layered sill: A key to the Karoo volcanics plumbing system. *Journal of Volcanology and Geothermal*  
788 *Research*, 172(1-2), 75-92.
- 789 MacLeod, C. J., Searle, R. C., Murton, B. J., Casey, J. F., Mallows, C., Unsworth, S. C., ... & Harris, M. (2009). Life  
790 cycle of oceanic core complexes. *Earth and Planetary Science Letters*, 287(3-4), 333-344.
- 791 O'Driscoll, B., Ferré, E. C., Stevenson, C. T., & Magee, C. (2015). The significance of magnetic fabric in layered  
792 mafic-ultramafic intrusions. In *Layered Intrusions* (pp. 295-329). Springer, Dordrecht.
- 793 Ondréas H., Cannat M., Fouquet Y., Normand A. Geological context and vents morphology of the ultramafic-hosted  
794 Ashadze hydrothermal areas (Mid-Atlantic Ridge 13N) // *Geochem. Geophys. Geosyst.* 2012.
- 795 Özdemir, Ö., & Dunlop, D. J. (1997). Effect of crystal defects and internal stress on the domain structure and  
796 magnetic properties of magnetite. *Journal of Geophysical Research: Solid Earth*, 102(B9), 20211-20224.

- 797 Pertsev AN, Aranovich LY, Prokofiev VY, Bortnikov NS, Cipriani A, Simakin SS, Borisovskiy SE (2015)  
798 Signatures of residual melts, magmatic and seawater-derived fluids in oceanic lower-crust gabbro from the Vema  
799 lithospheric section, Central Atlantic. *Journal of Petrology* 56(6): 1069-1088.
- 800 Pertsev AN, Bortnikov NS, Vlasov EA, Beltenev VE, Dobretsova IG Ageeva OA (2012) Recent massive sulfide  
801 deposits of the Semenov ore district, Mid-Atlantic Ridge, 13° 31' N: Associated rocks of the oceanic core complex  
802 and their hydrothermal alteration. *Geology of Ore Deposits* 54(5) :334-346.
- 803 Pertsev, A. N., Aranovich, L. Y., Prokofiev, V. Y., Solovova, I. P., Ageeva, O. A., Borisovskiy, S. E., Shatagin  
804 K.N., Zhilicheva, O. M. (2021). Potassium-rich granite melt inclusions in zircon from gabbro-hosted felsic stringers,  
805 Mid-Atlantic Ridge at 13° 34' N: E-MORB connection. *Lithos*, 106300.
- 806 Renne, P. R., Scott, G. R., Glen, J. M., & Feinberg, J. M. (2002). Oriented inclusions of magnetite in clinopyroxene:  
807 Source of stable remanent magnetization in gabbros of the Messum Complex, Namibia. *Geochemistry, Geophysics,*  
808 *Geosystems*, 3(12), 1-11.
- 809 Rochette, P., Jackson, M., Aubourg, C. Rock magnetism and the interpretation of anisotropy of magnetic  
810 susceptibility // *Reviews of Geophysics*. 30(3). P. 209-226. 1992
- 811 Rogers, J., Fox, J. M. W., & Aitken, M. J. (1979). Magnetic anisotropy in ancient pottery. *Nature*, 277(5698), 644-  
812 646.
- 813 Seifert, K. E. The genesis of plagioclase twinning in the Nonewaug granite // *American Mineralogist: Journal of*  
814 *Earth and Planetary Materials*. 49(3-4). P. 297-320. 1964
- 815 Selkin, P. A., Gee, J. S., & Meurer, W. P. (2014). Magnetic anisotropy as a tracer of crystal accumulation and  
816 transport, Middle Banded Series, Stillwater Complex, Montana. *Tectonophysics*, 629, 123-137.
- 817 Selkin, P. A., Gee, J. S., Meurer, W. P., & Hemming, S. R. (2008). Paleointensity record from the 2.7 Ga Stillwater  
818 complex, Montana. *Geochemistry, Geophysics, Geosystems*, 9(12).
- 819 Seront B., Mainprice D., Christensen N. I. A determination of the three-dimensional seismic properties of  
820 anorthosite: Comparison between values calculated from the petrofabric and direct laboratory measurements  
821 // *Journal of Geophysical Research: Solid Earth*. T. 98. №. B2. P. 2209-2221. 1993
- 822 Sobolev P (1990) Orientation of acicular iron-ore mineral inclusions in plagioclase. *International Geology Geology*  
823 *Review* 32(6).616-628
- 824 Stephenson, A. (1994). Distribution anisotropy: two simple models for magnetic lineation and foliation. *Physics of*  
825 *the Earth and Planetary Interiors* 82, 49–53.
- 826 Suhr G., Hellebrand E., Johnson K., Brunelli D. Stacked gabbro units and intervening mantle: A detailed look at a  
827 section of IODP Leg 305, Hole U1309D // *Geochemistry, Geophysics, Geosystems*. 9(10). 2008
- 828 Tan, W., Liu, P., He, H., Wang, C. Y., & Liang, X. (2016). Mineralogy and origin of exsolution in Ti-rich magnetite  
829 from different magmatic Fe-Ti oxide-bearing intrusions. *The Canadian Mineralogist*, 54(3), 539-553.
- 830 Tarduno, J. A., Cottrell, R. D., & Smirnov, A. V. (2006). The paleomagnetism of single silicate crystals: Recording  
831 geomagnetic field strength during mixed polarity intervals, superchrons, and inner core growth. *Reviews of*  
832 *Geophysics*, 44(1).

- 833 Tarling, D., Hrouda, F. (Eds.). Magnetic anisotropy of rocks. Springer Science & Business Media. 1993
- 834 Tauxe, L., Kodama, K. P., & Kent, D. V. (2008). Testing corrections for paleomagnetic inclination error in  
835 sedimentary rocks: a comparative approach. *Physics of the Earth and Planetary Interiors*, 169(1-4), 152-165.
- 836 Usui, Y., Nakamura, N., & Yoshida, T. (2006). Magnetite microexsolutions in silicate and magmatic flow fabric of  
837 the Goyozan granitoid (NE Japan): Significance of partial remanence anisotropy. *Journal of Geophysical Research:*  
838 *Solid Earth*, 111(B11).
- 839 Usui, Y., Shibuya, T., Sawaki, Y., & Komiya, T. (2015). Rock magnetism of tiny exsolved magnetite in plagioclase  
840 from a Paleoproterozoic granitoid in the Pilbara craton. *Geochemistry, Geophysics, Geosystems*, 16(1), 112-125.
- 841 Uyeda, S., Fuller, M. D., Belshe, J. C. & Girdler, R. W. (1963). Anisotropy of magnetic susceptibility of rocks and  
842 minerals. *Journal of Geophysical Research* 68, 279–291.
- 843 W.A. Deer, R.A. Howie, J. Zussman. An Introduction to the Rock-forming Minerals. Longman, London (1966), p.  
844 528.
- 845 Wack, M.R., Gilder, S.A. (2012). The SushiBar: an automated system for paleomagnetic investigations. *Geochem.*  
846 *Geophys. Geosyst.* 13, Q12Z38. <https://doi.org/10.1029/2011GC003985>.
- 847 Wack, M.R. (2015). Reliability of the AARM ellipsoid. In: Amer. Geophys. Union Fall Meeting, Abs. GP43A-  
848 1240.
- 849 Wenk HR, Chen K, and Smith R Morphology and microstructure of magnetite and ilmenite inclusions in plagioclase  
850 from Adirondack anorthositic gneiss // *American Mineralogist*. V. 96(8-9). P. 1316-1324. 2011
- 851 Xu, C., Zhao, S. R., Li, C., & He, X. (2016). Plagioclase twins in a basalt: an electron backscatter diffraction  
852 study. *Journal of Applied Crystallography*, 49(6), 2145-2154.
- 853 Xu, W., Geissman, J. W., Van der Voo, R., & Peacor, D. R. (1997). Electron microscopy of iron oxides and  
854 implications for the origin of magnetizations and rock magnetic properties of Banded Series rocks of the Stillwater  
855 Complex, Montana. *Journal of Geophysical Research: Solid Earth*, 102(B6), 12139-12157.



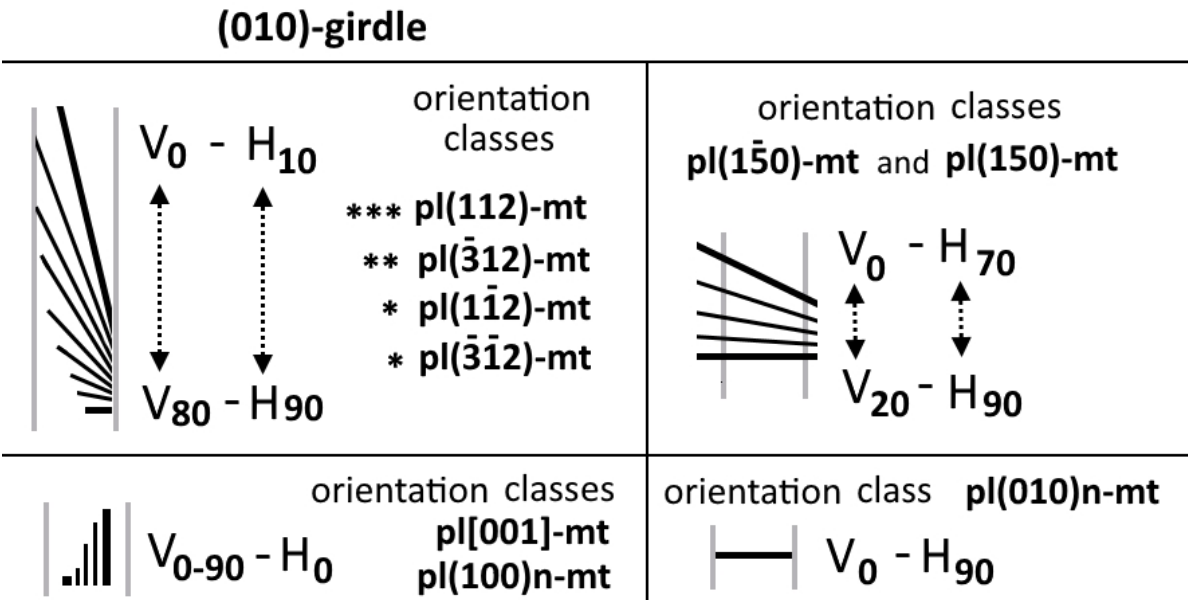
**SUPPLEMENTARY DATA**

Table T-1. sampling locations

dredge number	latitude, deg. N*	longitude, deg. W*	depth, mbsl*	geological structure
L2612	10.708	41.570	5195	Vema Transform Fault
L30-277	13.027	44.869	4089	OCC 13°N
L32-101	13.570	44.916	3407	OCC 13°30'N
1514	12.593	44.516	4116	Ashadze complex
1491	12.990	44.906	3300	Ashadze complex

\*dredge track start points

OCC – oceanic core complex (see text).



**Figure S-I.** Determination of the orientation classes in petrographic thin sections.

In cuts, where the albite twin boundaries are approximately perpendicular to the thin section plane the albite twin boundaries are very thin. In these sections the identification the different inclusion orientation classes that play a role in the formation of magnetic anisotropy is possible based on the angular relations of the magnetite needles with the plane of the albite twin boundary (vertical angle) and with the plane of the thin section cut (horizontal angle).

The needle-shaped magnetite micro-inclusions are represented by the black lines. The length of the lines is inversely proportional to the tilt of the inclusions relative to the surface of

the thin section. The cut with the albite twin boundary which is perpendicular to the thin section is represented by the vertical gray lines:

1. For the inclusions of  $pl(112)$ -mt,  $pl(-312)$ -mt,  $pl(1-12)$ -mt and  $pl(-3-12)$ -mt classes, the horizontal angle  $H=10^\circ$ , when the vertical angle  $V=0^\circ$ , and the horizontal angle  $H=90^\circ$ , when the vertical angle  $V=80^\circ$ . All possible orientations lie between these two orientations: the vertical (V) angle changes from  $0^\circ$  to  $80^\circ$ , the horizontal angle (H) changes from  $10^\circ$  to  $90^\circ$  (dashed lines with arrows). The angles H and V have positive correlation. The number of stars indicates the relative abundance of the orientation class of the micro-inclusions. The micro-inclusions belong to the (010)-girdle.

2. The  $pl(150)$ -mt and  $pl(1-50)$ -mt inclusions always are sub-horizontal with vertical angle (V) from  $0^\circ$  to  $20^\circ$ , and have a large horizontal angle (H) from  $70^\circ$  and  $90^\circ$  with the twin boundary. The angles H and V show positive correlation. The two types of the micro-inclusions often intersect the albite twin boundaries and are observed at about similar proportions.

3. The  $pl[001]$ -mt and  $pl(100)n$ -mt micro-inclusions are parallel to the albite twin boundaries ( $H=0^\circ$ ). They change vertical (V) angle from  $0^\circ$  to  $90^\circ$ . The  $pl[001]$ -mt class is more abundant than the  $pl(100)n$ -mt class. The micro-inclusions belong to the (010)-girdle.

4. The  $pl(010)n$ -mt micro-inclusions are rare in the plagioclase of oceanic gabbro. They are horizontal and perpendicular to albite twin boundaries ( $V=0$ ,  $H=90$ ).

Note, the image does not reveal the mutual orientations between the micro-inclusions. The angles are rounded to nearest ten.

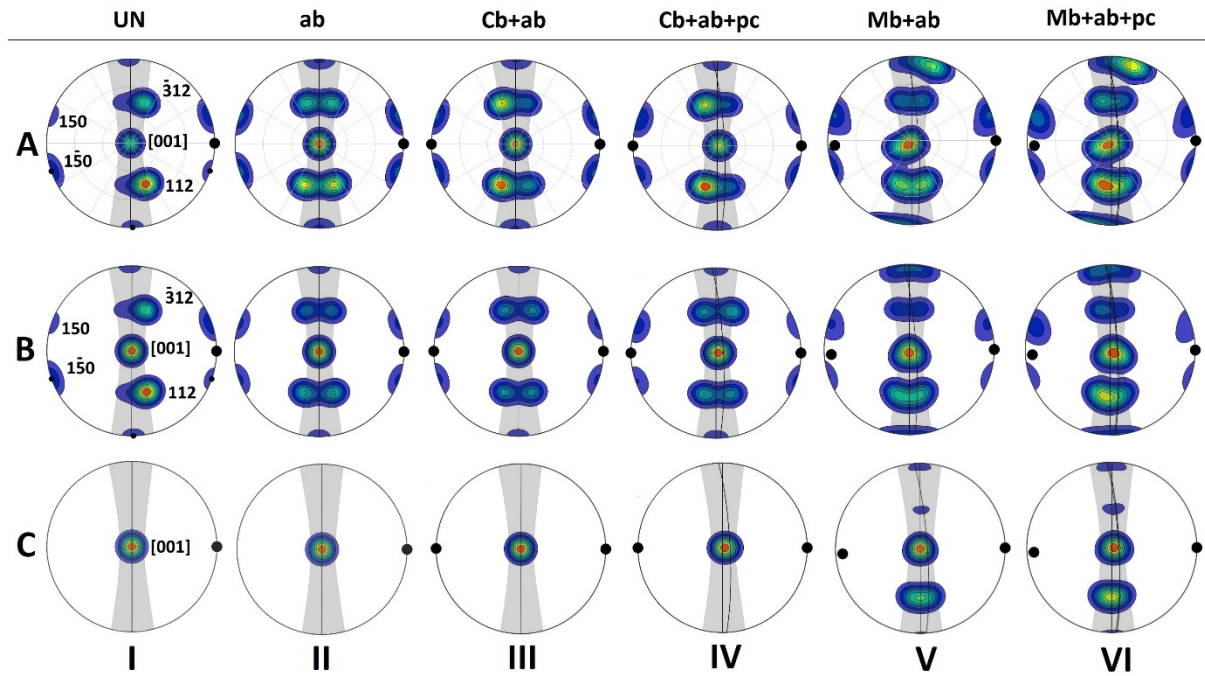


**Figure S-II.** Schematic plots of orientation distributions showing simulated statistical distributions (halfwidth 30 °) of the magnetite needle orientations in plagioclase with different combinations of twinning (Ab - Albite, p - pericline, Cb – Carlsbad, Mb – Manebach, UN - untwinned). In the first row (A) only the dominating “plane-normal” orientation class of magnetite micro-inclusions is considered. In the second row (B), both, the “plane-normal” and the pl[001]-mt orientation classes are considered. In the third row (C) only the pl[001]-mt orientation class is considered. The proportion of the inclusions pertaining to the different orientation classes are shown in Table 1. The 30°-girdle parallel to the pl(010) plane (gray areas) comprises the micro-inclusions oriented perpendicular to the pl(112), pl( $\bar{3}12$ ), pl(100), pl( $1\bar{1}2$ ), pl( $\bar{3}\bar{1}2$ ), and along the pl[001] direction.

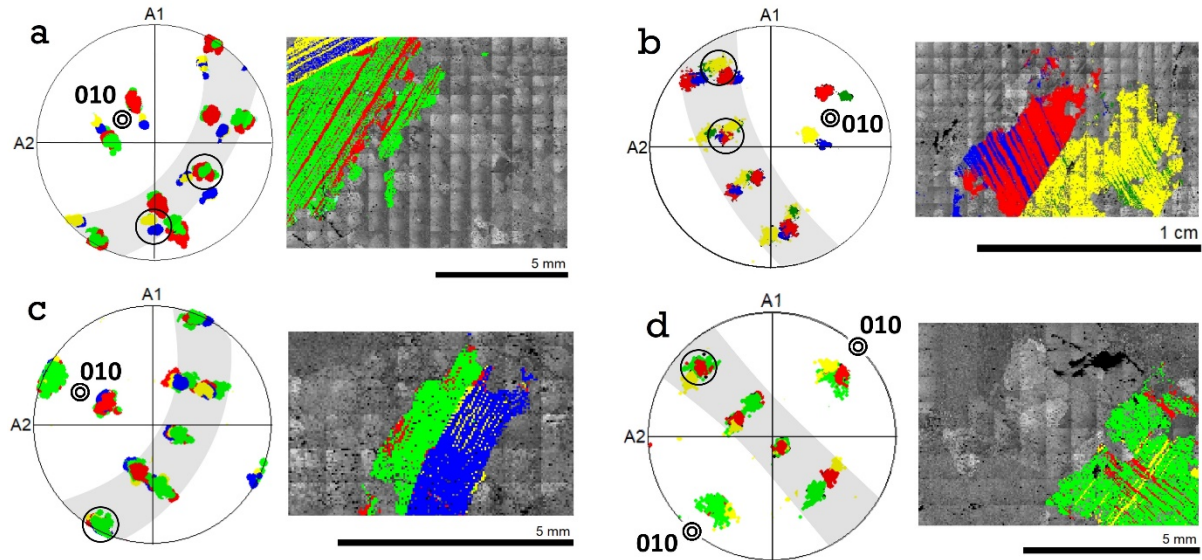
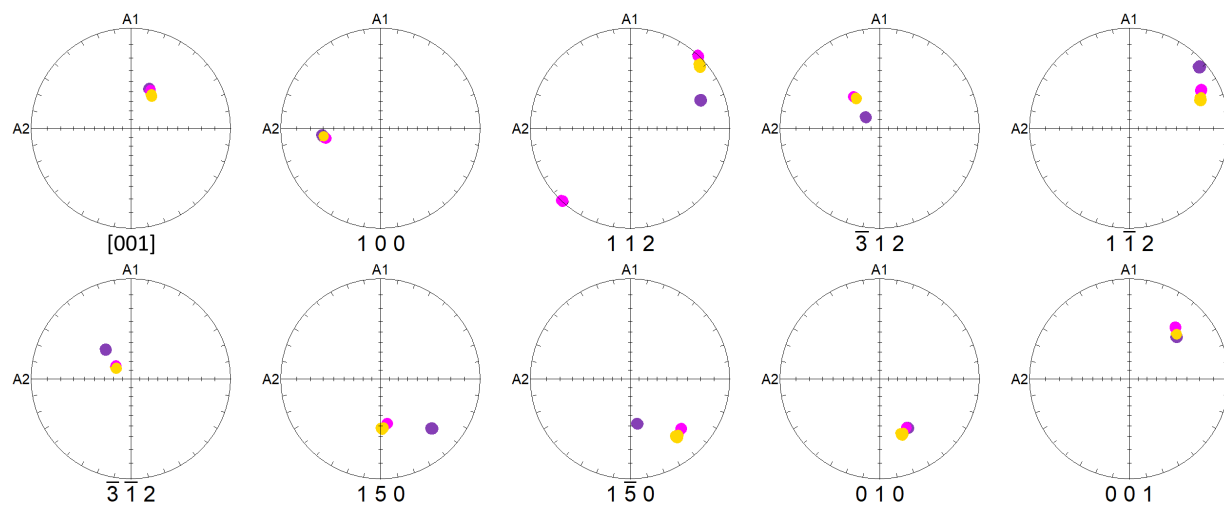


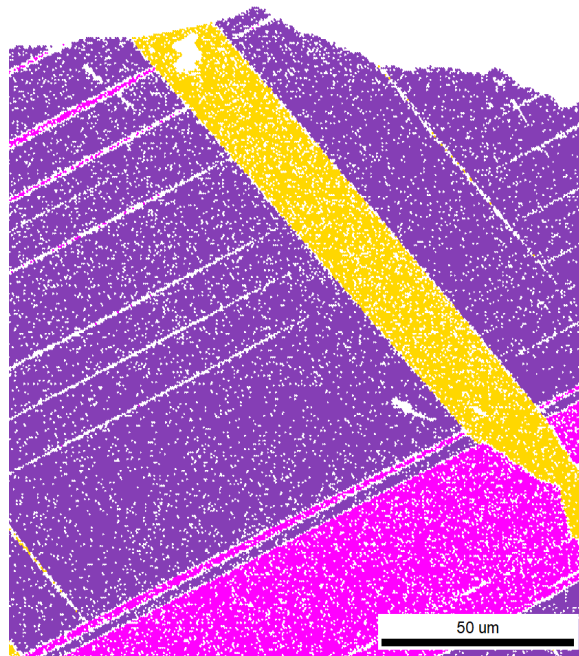
**Figure S-III.** Pole figures showing the poles of the plagioclase planes (EBSD data), which correspond to the elongation directions of the needle-shaped magnetite micro-inclusions of all eight orientation classes and orientation maps corresponding to these orientations. The plagioclase grains are twinned after the Manebach and Albite laws (a, b); Carlsbad and albite laws (c); and Pericline and Albite laws (d). The "30-degree girdles" containing the elongation directions of the majority of the oriented micro-inclusions are shaded in gray. The double circles indicate the poles of the pl(010) plane.

60

61



62

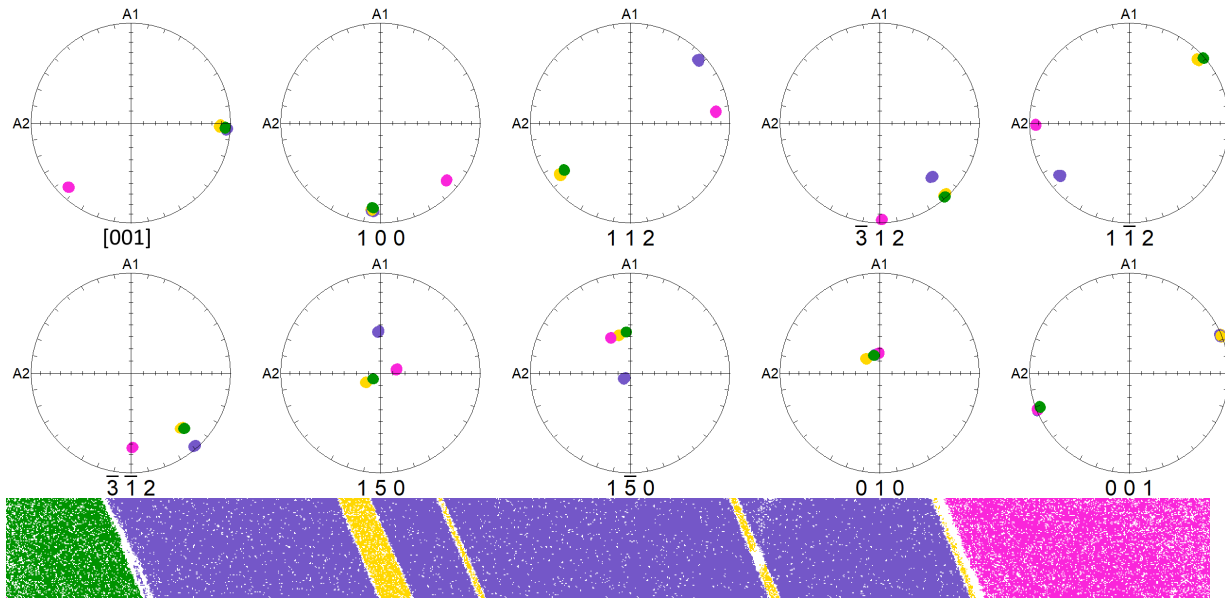


63

64

65

a.



b.

**Figure S-IV.** Stereographic projections (upper hemisphere) showing the poles of plagioclase lattice planes and directions including those corresponding to the elongation directions of the magnetite inclusions and planes, and orientation maps corresponding to these projections. (a) Sample 1514-17. The plagioclase grain is twinned after the Albite law (highlighted by purple and magenta colors) and by the Pericline law (yellow). See also Figure 9 (a- c). (b) Sample 1491-10. The plagioclase grain is twinned after the Manebach law. One Manebach twin is highlighted by magenta color, another one is twinned after the Pericline law (purple and yellow colors), and the Pericline + Albite law (green). See also Figure 9 (d- f).